Research Square

Preprints are preliminary reports that have not undergone peer review.
They should not be considered conclusive, used to inform clinical practice,
or referenced by the media as validated information.

Hybrid ANFIS-Based Fuzzy-PID Controller Design for Multi-Area Load Frequency Control in the Northwest Ethiopian Power Grid

Fekadu Gebey Moges
Girmaw Teshager Bitew
Yechale Amogne Alemu
Yechale.Amogne@inu.edu.et

Birhane Wondmaneh Getahun

Article

Keywords: Frequency deviation, load frequency control, PID controller, fuzzy-PID, ANFIS controller, ANFIS-based FPID

Posted Date: June 24th, 2026

DOI: https://doi.org/10.21203/rs.3.rs-9995293/v1

License: This work is licensed under a Creative Commons Attribution 4.0 International License.
Read Full License

Additional Declarations: No competing interests reported.

Hybrid ANFIS-Based Fuzzy-PID Controller Design for Multi-Area Load Frequency Control in the Northwest Ethiopian Power Grid

Fekadu Gebey Moges*[1], Girmaw Teshager Bitew[2], Yechale Amogne Alemu[3], and Birhane Wondmaneh Getahun[4]

[1,2]*Faculty of Electrical and Computer Engineering, Bahir Dar Institute of Technology (BiT), Bahir Dar University, Bahir Dar, P.O. Box 26, Ethiopia*

[3]*College of Engineering and Technology, Department of Electrical and Computer Engineering, Injibara University, Injibara, P.O. Box 40, Ethiopia*

[4]*College of Engineering and Technology, Department of Information Systems, Injibara University, Injibara, P.O. Box 40, Ethiopia*

fekadugebey630@gmail.com, gbitew1983@yahoo.com, Yechale.Amogne@inu.edu.et, Birhane.Wondmeneh@inu.edu.et

***Corresponding Author: Yechale.Amogne@inu.edu.et**

Abstract: The demand for electricity is rising daily, causing a mismatch between generation and demand and leading to frequency deviations from the nominal 50 Hz. Ethiopia's hydropower plants are interconnected to the national power grid and rely on primary load frequency control (LFC) mechanisms; however, a supplementary LFC mechanism is required to maintain system frequency centrally. This paper presents the design of a hybrid ANFIS-based fuzzy-PID (FPID) LFC scheme and compares its performance with those of a fuzzy-PID (FPID) controller, an adaptive neuro-fuzzy inference system (ANFIS)-based LFC controller, and the existing conventional PID controller within a three-area LFC model. The primary aim is to provide a robust and supplementary (centralized) LFC mechanism for the Ethiopian Electric Power grid that can replace the existing primary LFC mechanism and resolve the challenges associated with real-time tuning of PID parameters. The hydro-governor, hydraulic turbine, synchronous generator, tie-line, and load were modeled, followed by the formulation of a three-area LFC system model. The PID, FPID, ANFIS, and hybrid ANFIS-based FPID LFC controllers were designed in MATLAB/Simulink using three different governor models, and their performance metrics were evaluated comparatively. Changes in frequency and tie-line power flow, which together determine the area control error (ACE), serve as feedback signals to the governor for regulating water flow into the turbine. System response was assessed

in terms of overshoot, undershoot, steady-state error, and settling time under changes in system frequency and tie-line power flow. The proposed hybrid ANFIS-based FPID controller significantly outperforms the PID, FPID, and ANFIS controllers. In Scenario 1, the frequency deviation settling time was reduced to 12.959 s with an ITAE of 0.00565, compared to 48.8824 s and an ITAE of 0.0838 for the PID controller. Under multi-area disturbances (Scenario 2), the hybrid controller maintained its superiority with the lowest ITAE of 0.02375. Robustness analysis under ±25% parameter variations further confirmed its stability, with the ITAE remaining within the range of 0.00541 to 0.00580.

Keywords: Frequency deviation, load frequency control, PID controller, fuzzy-PID, ANFIS controller, ANFIS-based FPID.

1. Introduction

The frequency of a power system must remain close to its nominal value to ensure the reliable operation of equipment and frequency-sensitive loads. Deviations arise when demand and generation become imbalanced; a sharp frequency drop can cause excessive magnetizing current in motors and generators. Maintaining stable frequency is therefore vital for overall system performance [1]. An electrical power grid links multiple generating units from different stations through tie lines to balance load variations and meet demand. These tie lines enable bidirectional power exchange between interconnected systems and serve as the key regulation mechanism for maintaining grid stability [2].

Power systems consist of control areas, each representing a unified collection of generators that oscillate in synchronism and are characterized by consistent frequency deviations [3]. A significant control challenge in the operation of interconnected power systems is maintaining both frequency and inter-area power exchange at their designated values [4]. Load frequency control (LFC) is designed to provide regulation signals that modify the real power output of electrical generators within a specified area in response to variations in system frequency and

tie-line loadings, thereby ensuring compliance with the scheduled system frequency and the established power interchange with neighboring control areas [5].

In power system operation and control, LFC plays a major role in ensuring frequency stability. In an interconnected power system, all generators operate at the same frequency; any abrupt small load variation in one control area first causes the frequency of that area, and subsequently the transferred power of the tie lines, to deviate from their scheduled values [6]. To satisfy LFC objectives, a control signal known as the area control error (ACE) is measured, which represents the sum of net interchange power deviation and frequency deviation. Due to the static nature of PID gain values [7], emerging optimization techniques based on fuzzy logic, FPID structures, and artificial intelligence are increasingly applied to LFC and industrial automation for real-time parameter tuning. These techniques offer improved reliability, simplicity, and the ability to handle system nonlinearities [7].

The existing frequency control system of the Ethiopian power grid relies on a PID-based primary LFC mechanism, which is a classical controller whose parameters are difficult to tune in real time. Under extreme fault conditions and system disturbances, the plant and the National Load Dispatch Center (NLDC) require a more capable supplementary LFC mechanism. To address these power system frequency control challenges in interconnected power systems, FPID, ANFIS, and a hybrid ANFIS-based FPID LFC scheme are proposed as supplementary LFC mechanisms. The ANFIS-based FPID is a promising approach in which the fuzzy system is linked with PID for real-time tuning of the static PID parameters. This work also contributes to the Ethiopian electric power sector and to operators who currently rely on PID, by providing a system for real-time tuning and a supplementary LFC mechanism built upon the existing framework.

Testing controller performance in tuning the actual PID parameters and handling a three-area LFC model of the Northwest Region Ethiopian Electric Power (NWREEP) grid has important

implications for Ethiopia's transition from a conventional PID to a centralized control system. Currently, the country has an NLDC that continuously monitors the running status of each separate area, but load additions and rejections for frequency control action are handled by the primary PID-based LFC mechanism. The proposed approach is intended to apply a supplementary frequency control mechanism. An additional feature of this work is that controller performance was tested under three different governor models implemented in three distinct areas of the actual case study: a mechanical-hydraulic governor in Area 1, an electro-hydraulic governor in Area 2, and a PID-based electro-hydraulic HYGOV model in Area 3.

In summary, this paper addresses the challenges of the existing PID-based LFC mechanism in NWREEP, which requires a mechanism for real-time tuning of its static PID parameters and a supplementary, centralized LFC strategy. To alleviate these problems, the objectives of this study are: (i) mathematical modeling of a three-area LFC model and its system components; (ii) design of PID, FPID, ANFIS, and ANFIS-FPID controllers for the developed LFC model; (iii) comparative evaluation of the ANFIS-FPID controller performance against the alternatives; and (iv) validation of the robustness of the proposed controller under parameter variations.

2. Literature Review

Limon et al. [9] presented a Grey Wolf Optimization (GWO)-based fuzzy-PID controller for LFC in multi-area power systems. The proposed GWO-optimized cascaded fuzzy-PID controller, employing triangular membership functions, was evaluated on thermal-thermal and hybrid thermal-hydro-gas power systems. Controller parameters were tuned using the Integral Time Absolute Error (ITAE) objective function, which was also benchmarked against IAE, ISE, and ITSE criteria to ensure high precision in frequency stabilization. Performance metrics including ITAE, settling time, overshoot, and undershoot of frequency deviation as well as tie-line power deviation were evaluated. Robustness was established through sensitivity analysis

with ±50% variations in TG, TT, and TR parameters. Comparisons against controllers optimized using Modified Grasshopper Optimization (MGOA), Honey Badger Algorithm (HBA), Particle Swarm Optimization (PSO), Artificial Bee Colony (ABC), and Spider Monkey Optimization (SMO) demonstrated the superiority of the GWO-based fuzzy-PID approach.

Qu et al. [10] investigated multi-source power system LFC using Particle Swarm Optimization. The paper examined how integrating non-conventional energy sources affects tie-line power flow and system frequency. A PID controller for frequency regulation in both a one-area multi-source network (thermal, solar, wind, and fuel cells) and a two-area thermal interconnected system was proposed, with parameters optimized using PSO and ITAE as the objective function. Simulation results across different scenarios demonstrated that PSO-tuned PID outperforms conventional PID in frequency stabilization. The authors recommended exploring big data, cloud computing, and artificial intelligence as alternative optimization approaches for future LFC challenges.

Sokke Rameshappa and Shadaksharappa [11] proposed a neuro-fuzzy intelligent controller for LFC of a four-area power system, comparing ANFIS against conventional PID and Takagi-Sugeno-Kang fuzzy logic controllers with generation rate constraints on the turbine. A four-area power system combining thermal, hydro, and nuclear sources was modeled in MATLAB, and performance was assessed under step load changes using error, settling time, and maximum undershoot. The ANFIS controller outperformed both PID and fuzzy controllers by achieving lower peak deviations, faster settling, and eliminating steady-state error.

Gupta et al. [12] proposed load frequency control using a hybrid intelligent optimization technique for multi-source power systems. A two-area power system with thermal and hydro plants was modeled in MATLAB/Simulink, and performance under step load disturbances was evaluated using peak overshoot and settling time. The study recommended extending controller

tests to systems with more than two areas, applying varied load conditions, and incorporating parameter changes for broader validation.

Sharma [13] presented automatic generation control of a multi-source interconnected power system using ANFIS. In a two-area thermal-thermal interconnected system, output responses were evaluated using peak overshoot, undershoot, and settling time. The results showed that the PID controller is slower in correcting frequency and tie-line deviations, leading to the recommendation that intelligent controllers be adopted over classical ones for automatic generation control.

Precup et al. [14] provided a survey on fuzzy control for mechatronics applications, offering a structured overview of three pivotal directions in advanced fuzzy control theory. The review covers Takagi-Sugeno (T-S) fuzzy models for model-based control, data-driven fuzzy control for systems where accurate analytical models are difficult to obtain, and evolving fuzzy systems capable of online self-adaptation to changing dynamics. By illustrating each class with contemporary mechatronics applications, the survey substantiates their practical effectiveness. For the present work on multi-area LFC, this survey collectively justifies the pursuit of an ANFIS-based PID controller, as it employs a fuzzy inference structure amenable to stability analysis, leverages data-driven learning for adaptation, and aims to deliver robust performance in a nonlinear, stochastic power network.

In summary, ANFIS, ANFIS-based PI, and ANFIS-based PID controllers require a rule-based inference engine for real-time tuning of PID parameters. To harness the benefits of adaptability, learning capability, and rule-based reasoning, the proposed ANFIS-based FPID controller architecture offers a particularly viable solution. This architecture merges the computational intelligence of ANFIS with the robust, familiar structure of the existing PID. Consequently, for hydropower plant (HPP) control areas currently relying on PID-based LFC mechanisms, the integration of a rule-based optimization strategy is identified as a preferred approach for

achieving effective real-time parameter tuning and enhancing system stability. The proposed controller was tested under three different governor models representing Area 1 (mechanical-hydraulic), Area 2 (electro-hydraulic), and Area 3 (programmable PID-type electro-hydraulic governor).

3. Methodology

A three-area power system LFC model was developed with PID, FPID, and ANFIS-based FPID controllers for the case study area of the Northwest Region Ethiopian Power Grid. The model development began with data collection and analysis, supported by a concurrent literature review, followed by the mathematical modeling of the power system LFC components. Subsequently, a three-area LFC system model was formulated. After system modeling, the controllers were designed and tested in MATLAB/Simulink until each controller met the expected performance requirements.

3.1 Data Collection and Analysis

The data required to achieve the research objectives were obtained from the Ethiopian Electric Power (EEP) National Load Dispatch Center (NLDC) and are presented in the Appendix. All standard parameters used in system modeling and design are expressed in per-unit (p.u.) basis, with a base voltage of 400 kV and a base apparent power of 500 MVA (500 MW).

3.2 Modeling of Load Frequency Control System Components

Single- and multi-area hydropower systems, focusing on various components and their interconnections, were modeled and expressed using a transfer function approach.

3.2.1 Mathematical Modeling of the Hydraulic Turbine

The representation of the hydraulic turbine and water column in stability studies typically assumes negligible hydraulic resistance, an inelastic penstock pipe, and incompressible water [15]. The velocity of water varies directly with gate opening and with the square root of the net head, while the turbine output power is proportional to the product of head and volume flow.

The hydraulic plant, with a penstock-turbine system, includes an effective penstock length L, a water velocity U (ft/s) at discharge to the turbine, and a net head H, as depicted in Fig. 1.

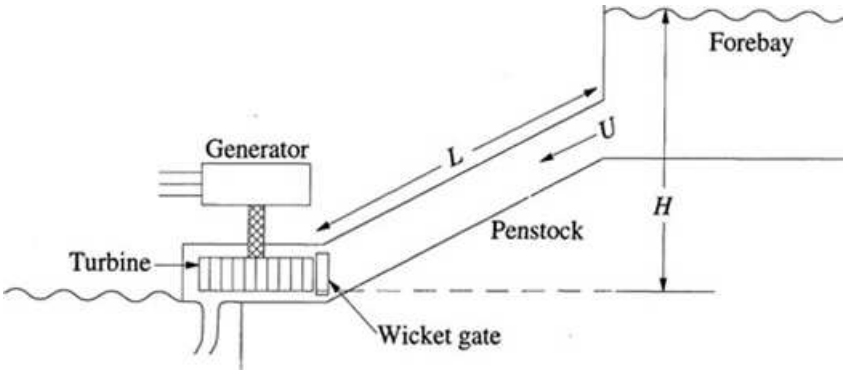


Fig. 1. Schematic diagram of a hydroelectric power plant.

The reduced first-order transfer function model for a hydraulic turbine system is expressed as given in (1), where Tw is the water time constant, ΔPm is the change in mechanical power of the turbine, ΔG is the gate position of the turbine water inlet distributor, s is the Laplace operator, and the negative sign indicates normalized values based on the steady-state operating condition.

3.2.2 Mathematical Modeling of the Hydro Governor

The main goal of a governor is to control speed and prevent drops in generator speed by using speed-error feedback to adjust the gate valve. These governors also incorporate droop characteristics to ensure stable operation of multiple generating units and can be mechanical-hydraulic, electro-hydraulic, or electrical/digital/programmable PID-type electro-hydraulic systems.

In the Northwest Region of the Ethiopian Electric Power plants, a PID-based electro-hydraulic governor is deployed at the Tana Beles Hydropower Plant (HPP), a PID-based mechanical-hydraulic governor is used at the Fincha Hydroelectric Power Plant, and an electrical, digital, and programmable PID-type electro-hydraulic governor is installed at the Tis Abay-2 Hydroelectric Power Plant. These three different governor types from the actual case study area

are used to test the controller performance. Fig. 2 shows the transfer function model of the electro-hydraulic governor with PID [13], where ΔPg is the input signal from the controller, ΔPc is the power output signal from the governor, TP is the pilot valve and servo time constant, Tg is the main governor (main servo) time constant, RP is the permanent droop constant, and Kp, Ki, and Kd are the proportional, integral, and derivative gains of the PID controller, respectively.

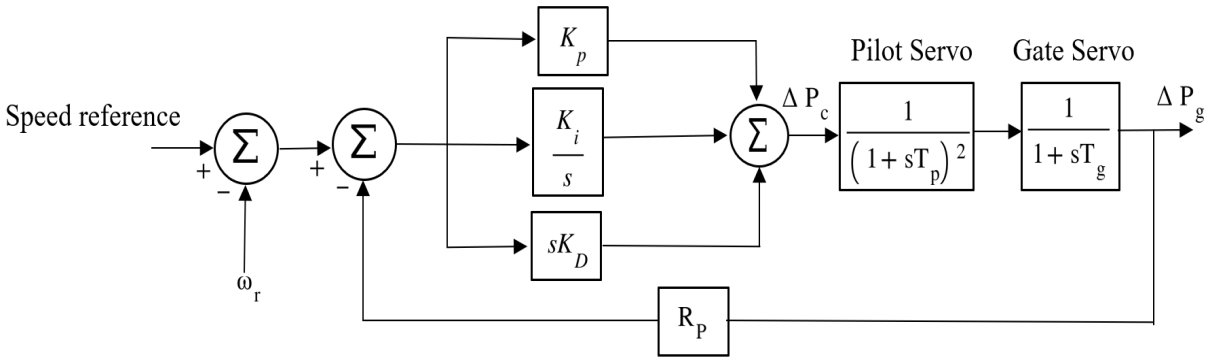


Fig. 2. Transfer function model of the electro-hydraulic governor with PID.

Fig. 3 shows the transfer function model of the mechanical-hydraulic governor of Fincha HPP with a PID-based mechanical-hydraulic governor transfer function, where ΔPc is the input signal from the controller, ΔPg is the power output signal from the governor, T1 is the speed governor reset time, T2 is the transient droop time constant, Tg is the main governor time constant, RT is the temporary droop constant, RP is the permanent droop constant, and H is the inertia constant of the synchronous generator in seconds. The values of T1, RT, and T2 are calculated as given in (2), (3), and (4), respectively.

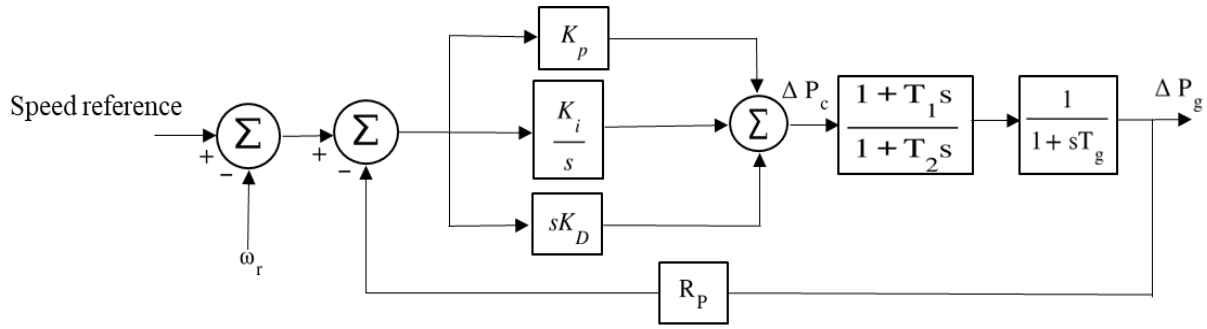


Fig. 3. Transfer function model of the mechanical-hydraulic governor of Fincha HPP with PID.

The turbine governor-penstock dynamics of the Tis Abay-2 HYGOV model represent a PID-based electro-hydraulic type hydro governor that depends on the permanent droop R (p.u. on generator MVA rating), transient droop r (p.u. on generator MVA rating), governor time constant Tr (s), filter time constant Tf (s), and main servo time constant Tg (s). Fig. 4 shows the transfer function representing the programmable PID-based electro-hydraulic HYGOV model of Tis Abay-2 HPP (Area 3). The final transfer function model representing the synchronous generator and load is given in Fig. 5, where ΔPm is the change in mechanical power, ΔPL is the change in load, H is the inertia constant, and D is the load damping constant.

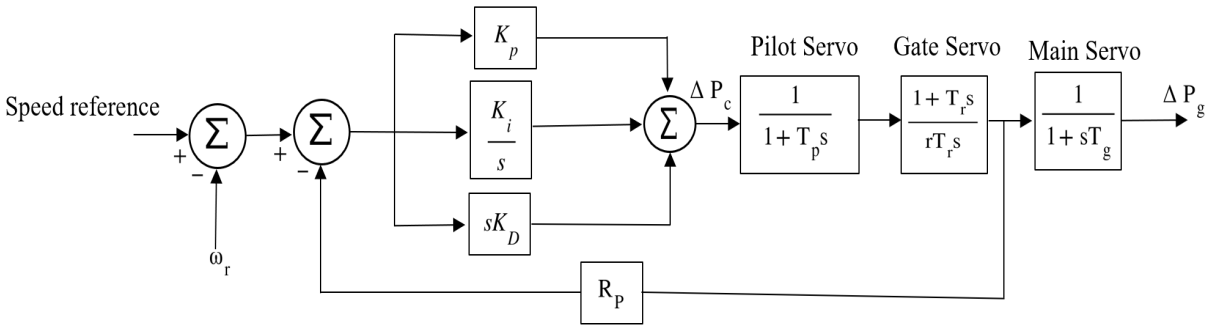


Fig. 4. Transfer function of the HYGOV Model Turbine-Governor Dynamics with PID controller for Tis Abay-2 HPP.

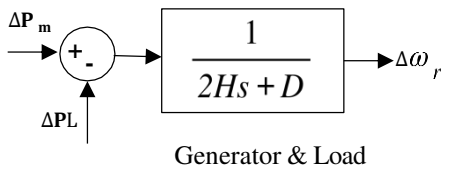


Fig. 5. Transfer function model of the synchronous generator and load.

3.3 Load Frequency Control Model of the Three-Area Power Grid

A multi-area power system consists of regions interconnected by high-voltage lines. The frequency trend in each control area reflects the overall power imbalance across the network, not just within a single area. Secondary frequency control (LFC) in the power grid is responsible for regulating both local frequency and tie-line power exchange. The relationship between interchange power, frequency deviation, and other parameters in an interconnected system with N control areas is illustrated in Fig. 6.

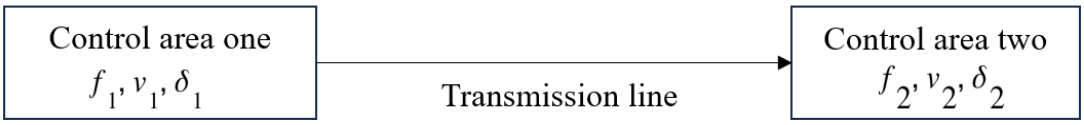


Fig. 6. Schematic representation of a two-area interconnected power system.

For modeling the N-area power system, consider first two areas represented by equivalent generating units interconnected by a lossless transmission line with reactance Xtie. The power transferred from control Area 1 to control Area 2 is given by (5), where P12 is the transferred power, X12 is the line reactance, δ12 is the power angle between the terminal voltages of the respective machines, and V1 and V2 are the terminal voltages of the equivalent machines.

At the initial operating condition, this is rewritten as (6). The incremental change in tie-line power is obtained by differentiating (6) with respect to δ12 and evaluating at the initial condition, yielding (7). Linearizing (7) about an equilibrium point δ10, δ20 gives (8), where T12 is the synchronizing torque coefficient defined as the differential power increase per differential power angle increase, given by (9). Differentiating and taking the Laplace transform of (8) gives (10) and (11). By considering the relationship between area power angle and frequency and substituting, the tie-line power deviation between Area 1 and Area 2 is expressed in (12). The Laplace transform of the tie-line power deviation between Areas 1 and 2 is given in (13), and corresponding expressions for Areas 1-3 and Areas 2-3 are given in (14) and (15), respectively.

The total tie-line power change for one area with respect to all N control areas is computed by (16), and the net tie-line power deviation for the three-area power plant is given by (17). As a result of the net tie-line power deviation within the power grid system, the composite frequency characteristics β for the three-area power system can be expressed mathematically as (18), where β1, β2, and β3 are the frequency response characteristic factors for Areas 1, 2, and 3, respectively.

The control signal generated by combining tie-line power flow deviations with frequency deviations weighted by a bias factor yields the area control error (ACE). The ACE signal, which is the input to the gate or valve controllers, is vital for maintaining frequency at scheduled values and permissible limits, and for maintaining net interchange power with neighboring areas at scheduled values. The ACE for a given control area is given by (19), and the general expression for the ACE of the ith control area is given by (20), where ACE1, ACE2, and ACE3 correspond to control Areas 1, 2, and 3, respectively. The three-area interconnected hydropower LFC system model utilizing transfer function representation is shown in Fig. 7, representing Tana Beles (Area 1), Fincha (Area 2), and Tis Abay-2 (Area 3).

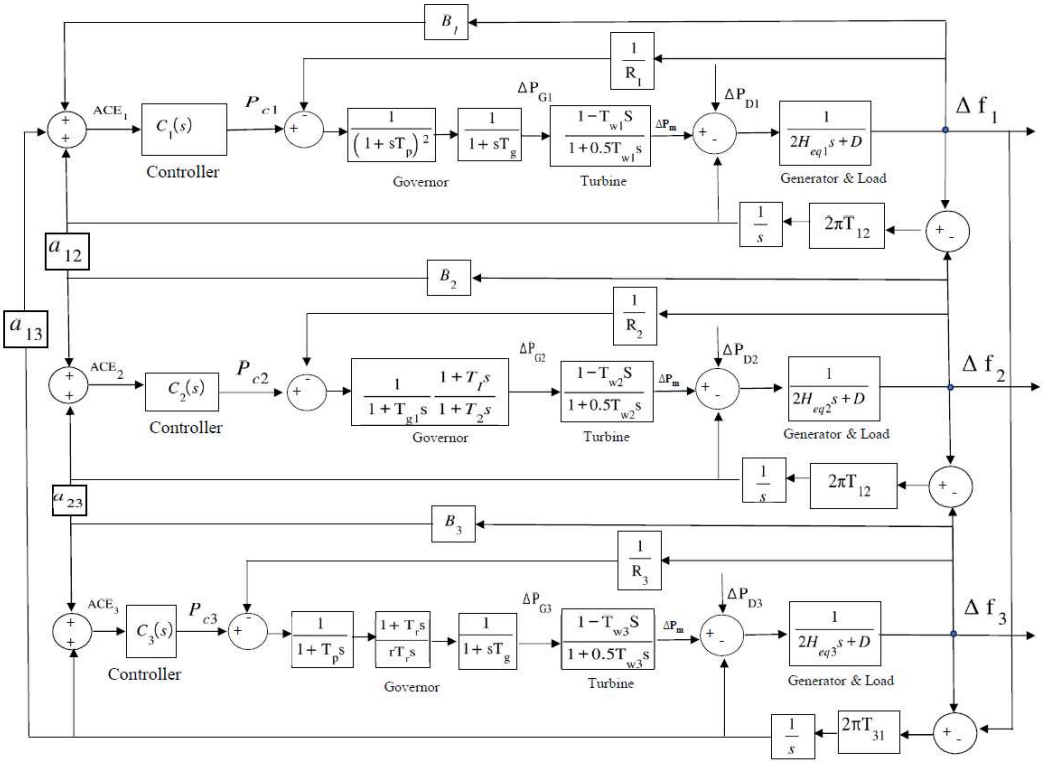


Fig. 7. Three-area interconnected HPS LFC system model.

3.4 Controller Design for the Three-Area Power System

PID is a static controller, whereas power systems are dynamic and time-varying, making static PID controllers less effective. The PID controller is mathematically represented as given in (21), where PIDout denotes the controller output, Kp is the proportional gain, Ki is the integral gain, Kd is the derivative gain, e is the error (the difference between the actual value and the set point), and t is the instantaneous time in seconds. For LFC of a power grid, this expression is rewritten in terms of the ACE as given in (22), and the PID controller outputs for the three-area power grid are expressed in (23).

PID tuning was performed using the Ziegler-Nichols sustained oscillation method [7], following the procedure outlined below:

- Apply a step load change without any controller.
- Insert the PID controller and set only Kp while Kd and Ki are set to zero.

- Increase Kp until sustained oscillations are achieved and the critical gain Kcr is reached.
- Measure and record Kcr and Pcr, then compute Kp, Ki, and Kd using the Ziegler-Nichols formulae.

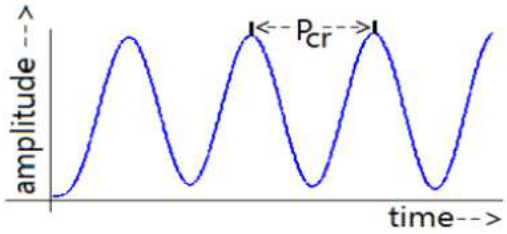


Fig. 8. PID parameter tuning using the Ziegler-Nichols sustained oscillation method [7].

Table 1. Ziegler-Nichols formulae — sustained oscillation method.

Controller	Kp	Ki	Kd
PID	0.6Kcr	½Pcr	⅛Pcr

3.4.1 Design of the FPID-Based LFC Controller

The FPID design methodology began by developing a dynamic model for the three interconnected power areas with PID and establishing a performance baseline by setting conventional PID controller gain ranges for each area. A hybrid structure was then defined in which a fuzzy logic system dynamically adjusts the baseline PID gains (Kp, Ki, Kd) in real time. The ACE and its rate of change (ΔACE) serve as the two crisp inputs to the fuzzy system, with five linguistic variables: Negative Big (NB), Negative Small (NS), Zero (Z), Positive Small (PS), and Positive Big (PB), using triangular membership functions and a Mamdani fuzzy inference engine. The FPID controller was developed with 25 fuzzy rules loaded via a .fis file into the MATLAB Fuzzy Toolbox. The system was then tuned systematically until the minimum ITAE was obtained.

Fig. 9 shows the schematic diagram of the LFC system using the FPID controller. Tables 2, 3, and 4 present the fuzzy rule base tables for the proportional gain Kp, integral gain Ki, and derivative gain Kd, respectively.

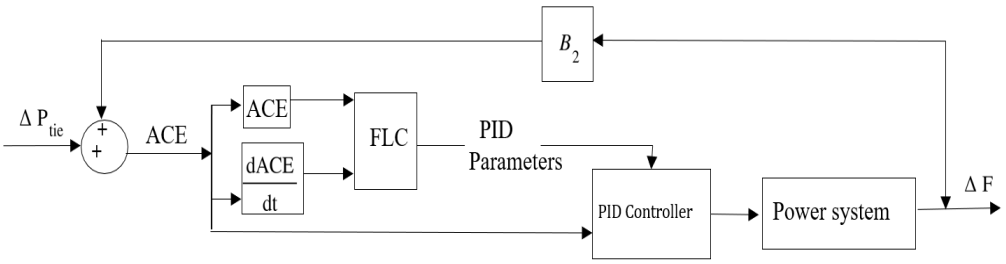


Fig. 9. Schematic diagram of the LFC system using the FPID controller.

Table 2. Fuzzy rule base table for proportional gain Kp.

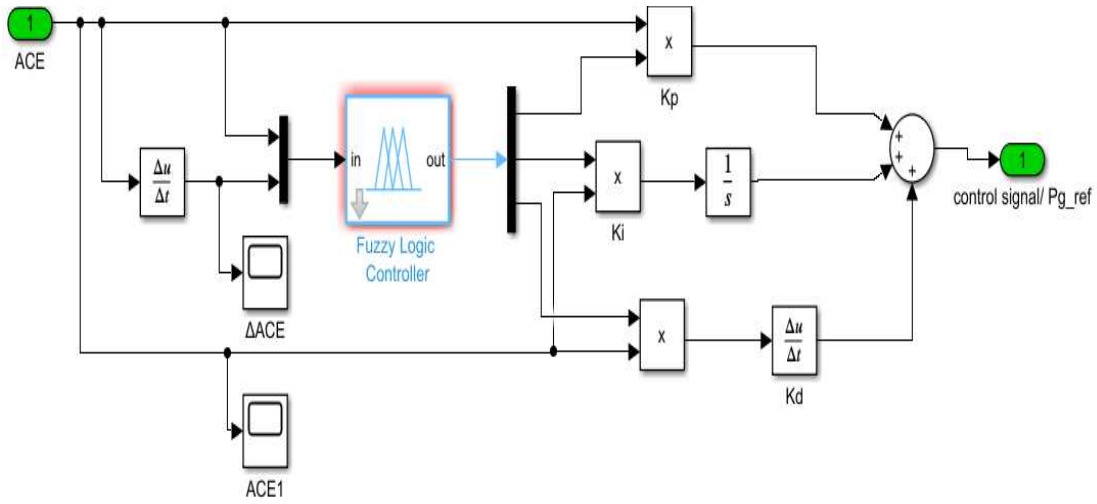
ACE \ ΔACE	NB	NS	Z	PS	PB
NB	PB	PB	PB	PB	PB
NS	PS	PS	PS	Z	PB
Z	NB	NB	NB	NS	NS
PS	PS	PS	PS	Z	PB
PB	PB	PB	PB	PB	PB

Table 3. Fuzzy rule base table for integral gain Ki.

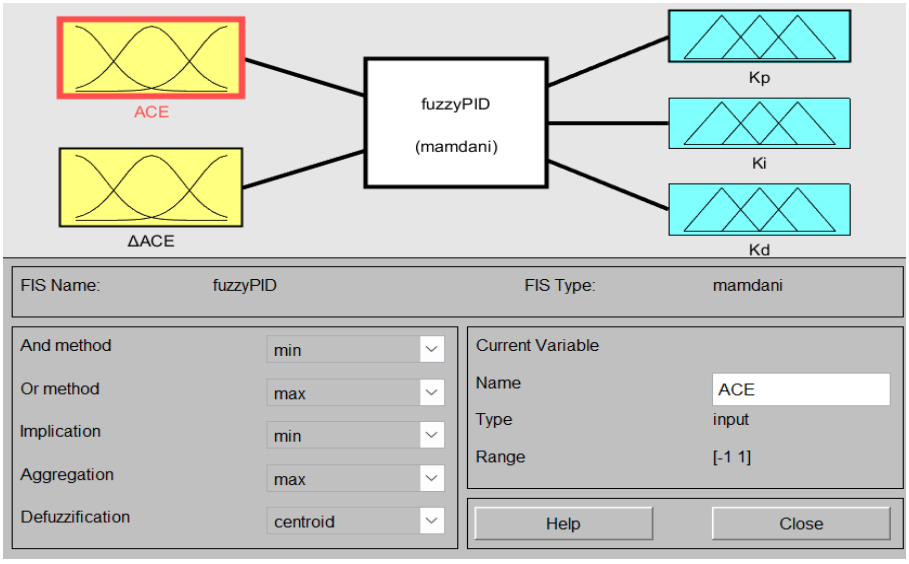
ACE \ ΔACE	NB	NS	Z	PS	PB
NB	Z	Z	Z	Z	Z
NS	NS	NS	NS	NS	NS
Z	NS	NS	NB	NS	NS
PS	NS	NS	NS	NS	NS
PB	Z	Z	Z	Z	Z

Table 4. Fuzzy rule base table for derivative gain Kd.

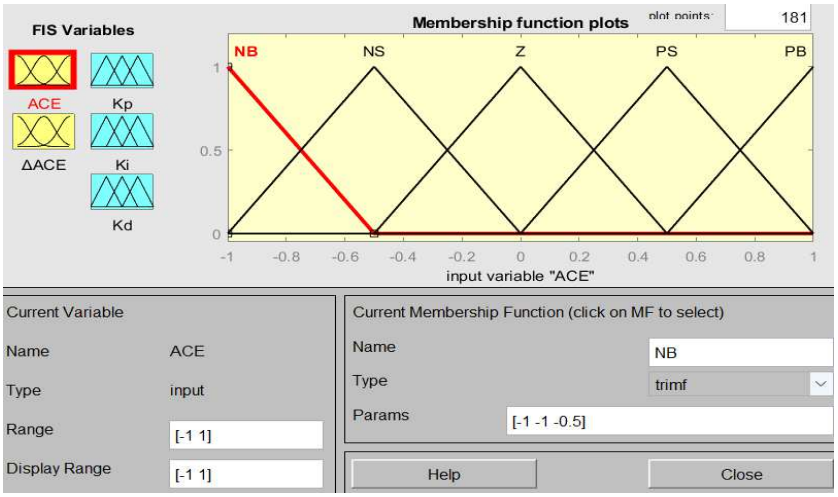
ACE \ ΔACE	NB	NS	Z	PS	PB
NB	NB	NS	Z	Z	PB
NS	NS	PS	Z	PB	PB
Z	Z	Z	Z	PB	PB
PS	PS	PB	PB	PB	PB
PB	PB	PB	PB	PB	PB



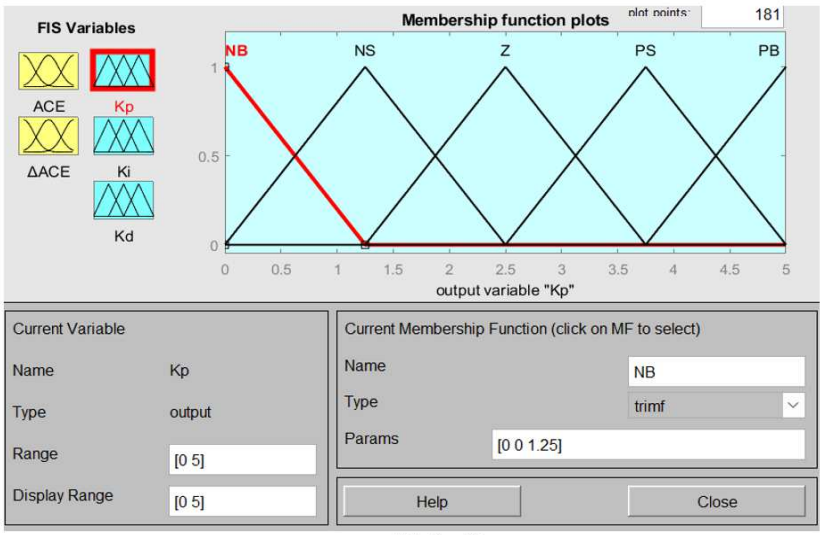
(a). MATLAB Simulink diagram of FPID controller.



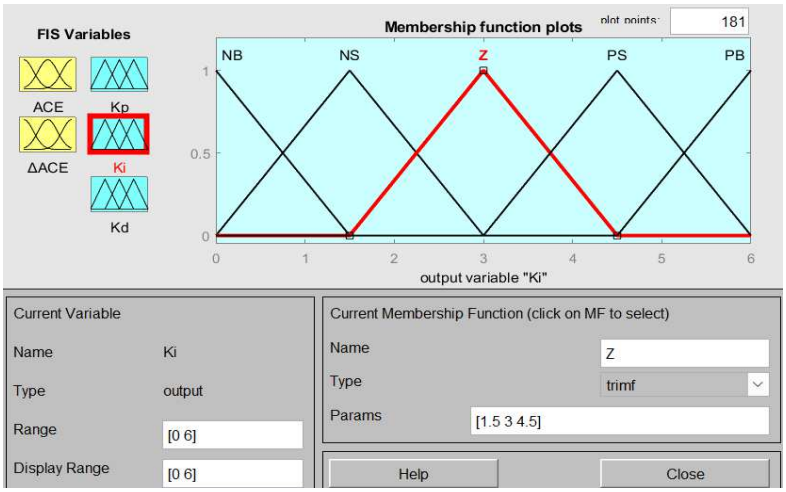
(b). Membership function showing crisp inputs and crisp outputs



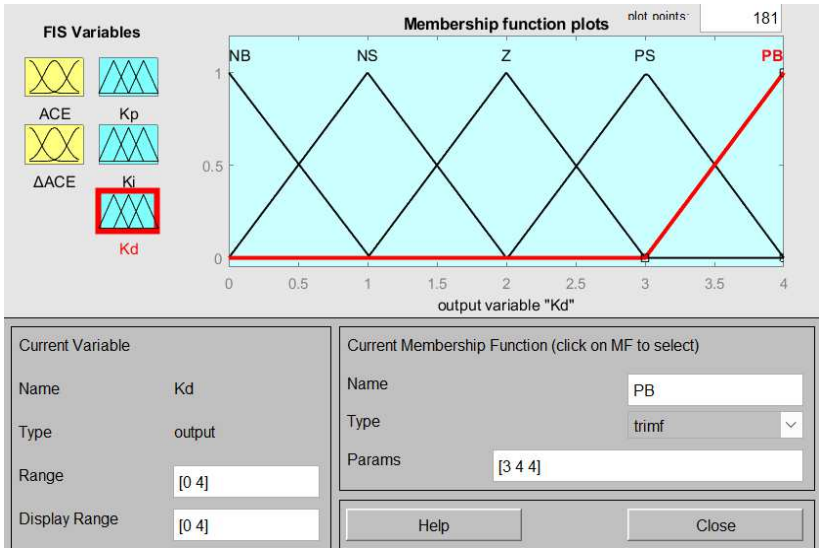
(c). Membership function showing ACE and ΔACE



(d) membership function for K_d



(e) membership functions for K_i



(f) membership functions for K_d

Fig. 10: structure of the fuzzy rules and membership functions of FPID LFC model

3.4.2 Design of the ANFIS-Based LFC Controller

A neuro-fuzzy system combines neural networks and fuzzy logic to learn parameters from data. It automatically creates a fuzzy rule base and membership functions, making it effective for modeling complex relationships. ANFIS is widely used in system identification and time series prediction, offering the interpretability of fuzzy systems along with the learning power of neural networks. Among fuzzy inference systems, the Sugeno-type is preferred in LFC for its computational efficiency in evaluating unknown parameters and for its many-inputs-to-one-output structure.

The Sugeno fuzzy rule Rk is stated as given in (24), where the antecedent membership functions map the inputs to fuzzy sets, and the consequent parameters are tuned during training by the ANN component. Membership functions, which describe the degree to which a given input belongs to a set, can be triangular, trapezoidal, or Gaussian in shape. In this work, triangular membership functions are used for the fuzzy system [17], while Gaussian membership functions are employed in the ANFIS, as described in (25).

The transfer function of an electro-hydraulic governor, like all transfer functions, is a linear mathematical tool that represents a linearized model of a fundamentally nonlinear physical system [18],[19]. ANFIS addresses this by adapting to system changes (e.g., load variations, generation capacity changes) through time-varying parameters. The ANFIS used in the LFC MATLAB simulations represents a non-linear, practical power system that accounts for non-ideal operational uncertainties inherent in real-world multi-area power grids but abstracted in canonical linear models. In contrast to a linear PID with static gains (Kp, Ki, Kd), the ANFIS framework continuously adjusts the effective gains of the PID structure based on the system's real-time error and its rate of change, making it an excellent candidate for LFC in multi-area power systems.

3.5 LFC of the Multi-Area Power System Using ANFIS

ANFIS can effectively regulate the reference value of the governor under various governor models. Since power system load continuously varies, the governor must handle these variations and track its regulation according to the power reference signal (i.e., the control signal output of the ANFIS controller). Here, the ACE and its derivative are used as inputs, and the power reference signal is used as the output. Fig. 11 shows the ANFIS structure of the LFC, and Fig. 12 shows the architecture of the ANFIS, where Layer 1, Layer 2, Layer 3, Layer 4, and Layer 5 are the fuzzification, implication/product, normalizing, defuzzification, and output/summation layers, respectively.

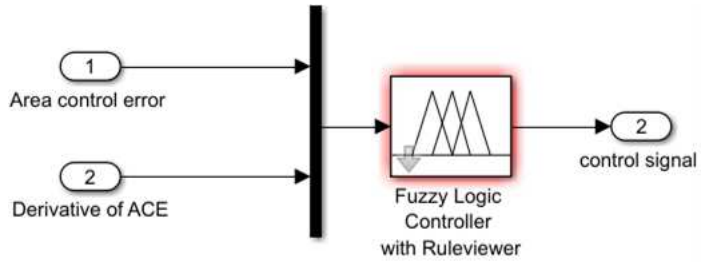


Fig. 11. ANFIS structure of the LFC

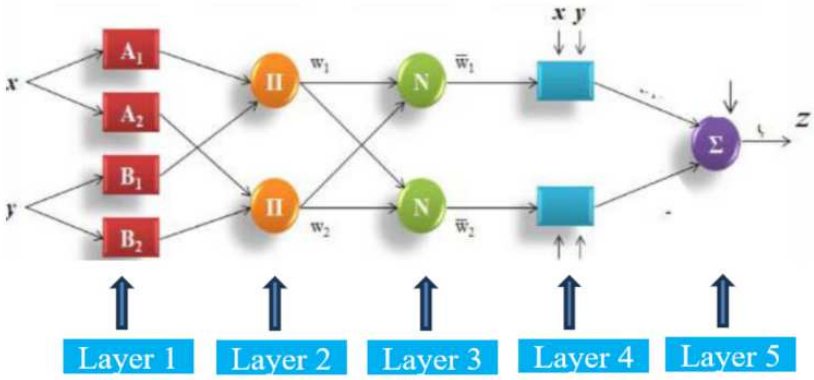


Fig. 12. Architecture of the ANFIS.

3.6 Algorithm for Deploying ANFIS

The ANFIS training steps for the design of the ANFIS-based LFC are presented as follows:

1. Step 1: Test the system with PID.
2. Step 2: Collect training data (ACE, ΔACE, and output) while simulating the model with PID.

3. Step 3: Use the ANFIS editor tool in the MATLAB/Simulink environment to generate a .fis file.
4. Step 4: Arrange the training data collected in Step 2 column-wise and generate the .fis file. The first column is ACE, the second is ΔACE (inputs), and the third column is the output.
5. Step 5: Assign the number and type of membership functions, optimization method, and error tolerance appropriately.
6. Step 6: Train the collected data with the generated .fis for up to 100 epochs.
7. Step 7: Save the .fis file. This file constitutes the neuro-fuzzy enhanced ANFIS model.

The training data were obtained from simulation-based sources. Specifically, training data extracted when the system was run with PID under a given load disturbance were used for ANFIS performance evaluation under the same disturbance condition.

When running the system with PID, a total dataset of no fewer than 783 input-output pairs was generated from system simulations across different scenarios and systematically partitioned for training, testing, and validation. Of this data, 70% (approximately 548 samples) was allocated for training, during which the ANFIS algorithm iteratively adjusted the antecedent and consequent parameters to minimize the error between the model's predicted control signal and the desired optimal control signal. To prevent overfitting, a separate testing set comprising 15% of the data (approximately 117 samples) was used. Finally, a distinct validation set of the remaining 15% (another 117 samples) provided an unbiased assessment of model generalization capability after training. The Root Mean Square Error (RMSE) calculated on the validation set provides a clear measure of how effectively the trained ANFIS model will perform when deployed.

3.7 Design of the ANFIS-Based FPID Controller

The hybrid controller integrates the advantages of both ANFIS and FPID. The FPID component ensures robust and adaptive real-time control, while the ANFIS component improves accuracy by learning from system performance and adjusting its fuzzy rules accordingly. By combining both controllers, the overall performance of the LFC system is improved, addressing nonlinearities, uncertainties, and the need for adaptive control. Fig. 13 shows the ANFIS-based FPID LFC model.

The design methodology for the ANFIS-based FPID directly combines the training steps and design procedures of the ANFIS and FPID controllers. As shown in Fig. 13, the trained, optimized, and enhanced ANFIS controller output during simulation is taken as the ACE; this error and its derivative are then fed as inputs to the FPID controller. The governor input reference power signal is determined by the combined output of both the ANFIS and FPID controllers.

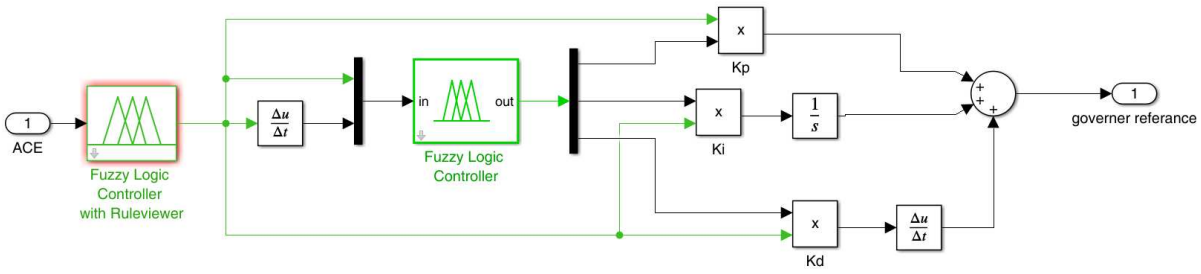


Fig. 13. ANFIS-based FPID LFC model.

3.8 Objective Function for the Optimization Problem

The global objective function of the LFC problem aims to minimize the fitness function, which is a minimization problem of the ITAE performance index subject to the constraints given in (26) and (27). The gain ranges are [0, 5], [0, 6], and [0, 4] for Kp, Ki, and Kd, respectively, for Areas 1 and 2, and [0, 3], [0, 8], and [0, 5] for Kp, Ki, and Kd, respectively, for Area 3, where the superscripts min and max denote the minimum and maximum variable values, ΔF1, ΔF2, and ΔF3 are the system frequency deviations, ΔPtie1, ΔPtie2, and ΔPtie3 are the incremental

tie-line power flow changes, and tsim is the simulation time horizon. Fig. 14 shows the MATLAB/Simulink model of the objective function.

Performance specifications including ITAE, overshoots, and undershoots are enforced primarily through the objective function during the training and tuning phases. A data-driven specification imposition approach is also applied: during ANFIS training, the iterative process is repeated until minimal overshoot, undershoot, and ACE elimination are achieved. Changes in frequency and tie-line power (increments or decrements) are fed back to the controller as ACE and its derivative, and the controller takes action according to the fuzzy and ANFIS rule sets.

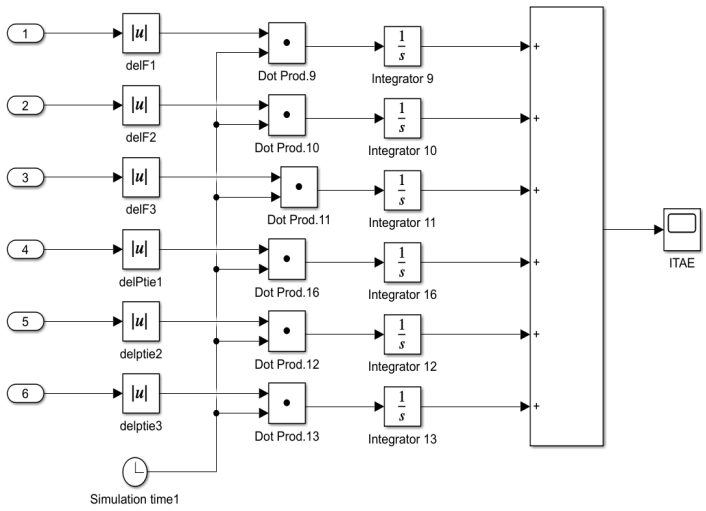


Fig. 14. Objective function of the optimization problem in MATLAB/Simulink.

3.9 Multi-Area LFC System MATLAB/Simulink Model

Fig. 15 shows the multi-area LFC model in the MATLAB/Simulink environment, where B1, B2, B3 are the frequency bias factors; R1, R2, R3 are the self-regulation parameters of the governor in p.u.; Tg1, Tg2, and Tg3 are the speed governor (main servo) time constants; and T12, T13, and T23 are the transmission line synchronizing coefficients.

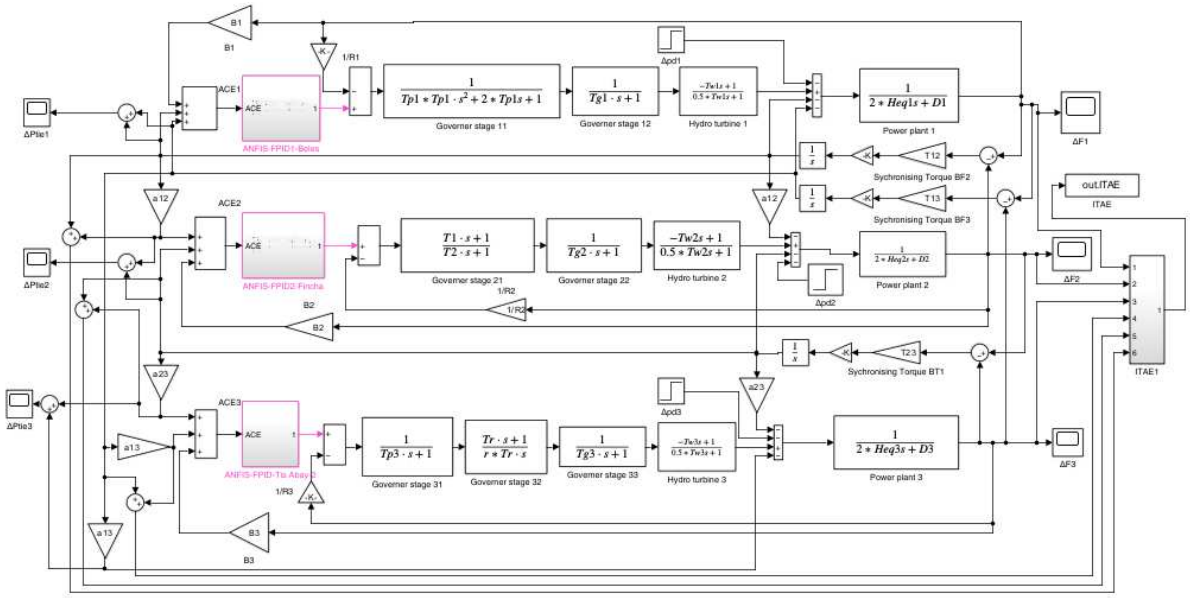


Fig. 15. Multi-area LFC model in MATLAB/Simulink.

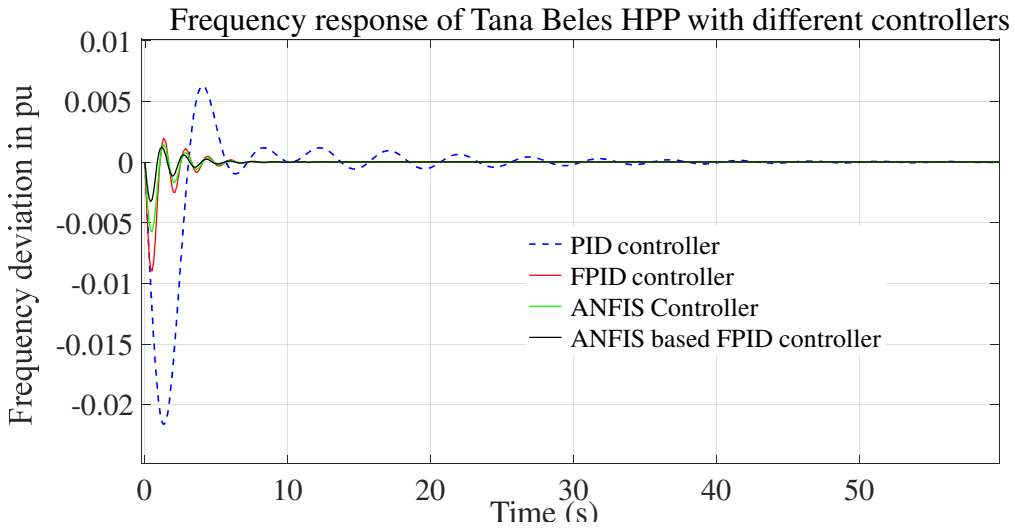
4. Simulation Results and Discussion

The proposed LFC system was simulated in MATLAB/Simulink for a duration of 60 s. Load disturbances were introduced to assess the transient and steady-state performance of the four controllers: conventional PID, FPID, ANFIS, and the proposed hybrid ANFIS-FPID. Controller performance was evaluated using settling time, peak overshoot, and peak undershoot, with ITAE as the primary performance criterion. Three main scenarios were considered:

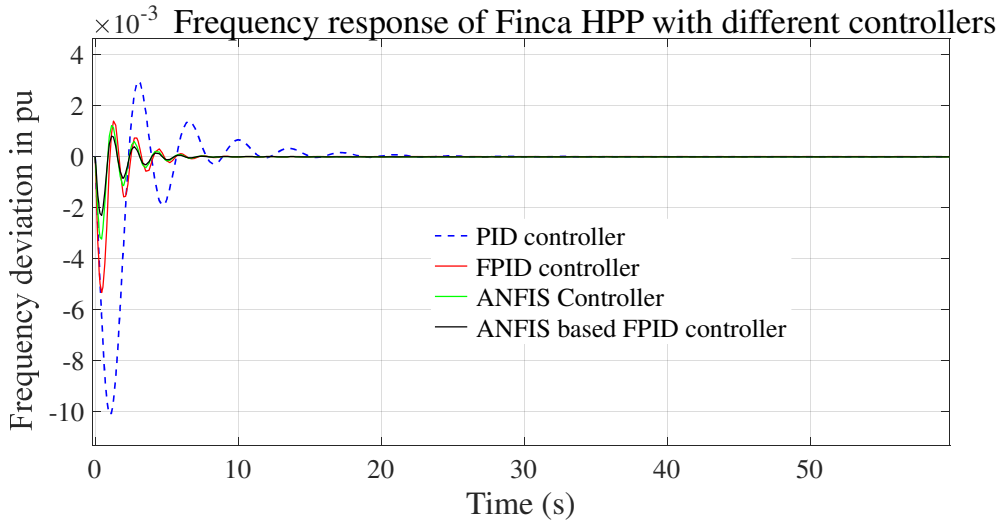
- Scenario 1: A load disturbance of 0.01 p.u. applied in Area 1 only.
- Scenario 2: Simultaneous load disturbances of 0.46 p.u., 0.0268 p.u., and 0.016 p.u. in Areas 1, 2, and 3, respectively (representing 50% load variation in Area 1 and 10% in Areas 2 and 3).
- Scenario 3: Sensitivity (robustness) analysis under ±25% variation of selected system parameters.

4.1 Load Disturbance in Control Area 1 Only

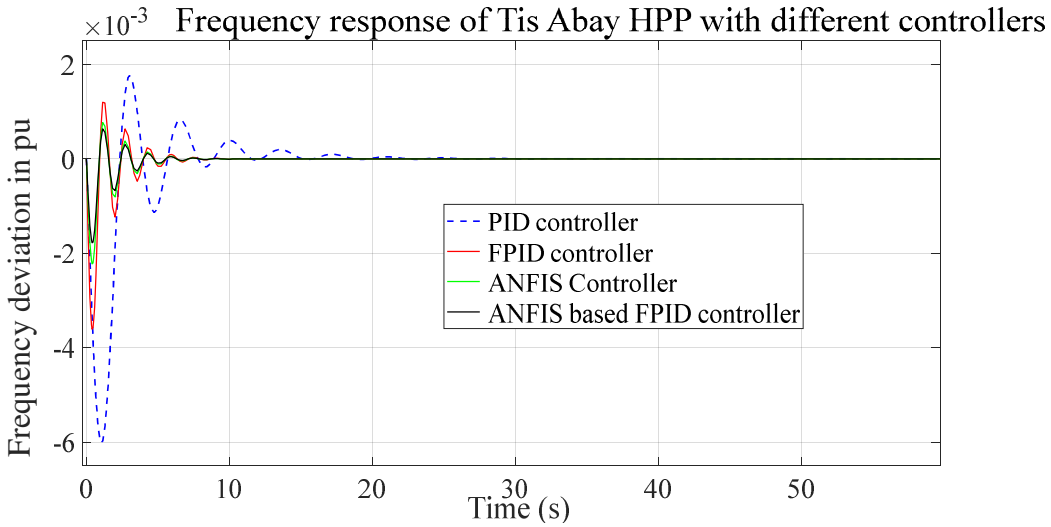
Under Scenario 1, a unit load perturbation (ΔPD1 = 0.01 p.u.) was applied to Area 1. Fig. 16 presents the frequency deviation responses of the three areas for each controller, and the corresponding settling time, peak overshoot, and peak undershoot values are summarized in Table 5.



(a). area-1



(b). area-2



(c). area-3

Fig. 16: Frequency deviation responses in p.u for load change in area one only

Table 5. Comparative analysis of frequency deviation responses for a load perturbation in Area 1 only.

Controller	Performance parameter	ΔF_1	ΔF_2	ΔF_3	ITAE
PID	Peak overshoot (pu)	0.00628	0.00290	0.00176	0.0838
	Peak undershoot (pu)	-0.02162	-0.01014	-0.00601	
	Settling time (s)	48.8824	34.084	32.983	
FPID	Peak overshoot (pu)	0.00197	0.00140	0.00119	0.02636
	Peak undershoot (pu)	-0.00898	-0.00534	-0.00361	
	Settling time (s)	13.479	13. 246	13.136	
ANFIS	Peak overshoot (pu)	0.001448	0.00122	0.00078	0.00932
	Peak undershoot (pu)	-0.005735	-0.00317	-0.00223	
	Settling time (s)	13.015	12.870	12.093	
ANFIS -FPID	Peak overshoot (pu)	0.001243	0.00081	0.00064	0.00565
	Peak undershoot (pu)	-0.00325	-0.00231	-0.00178	
	Settling time (s)	12.959	11.927	11.283	

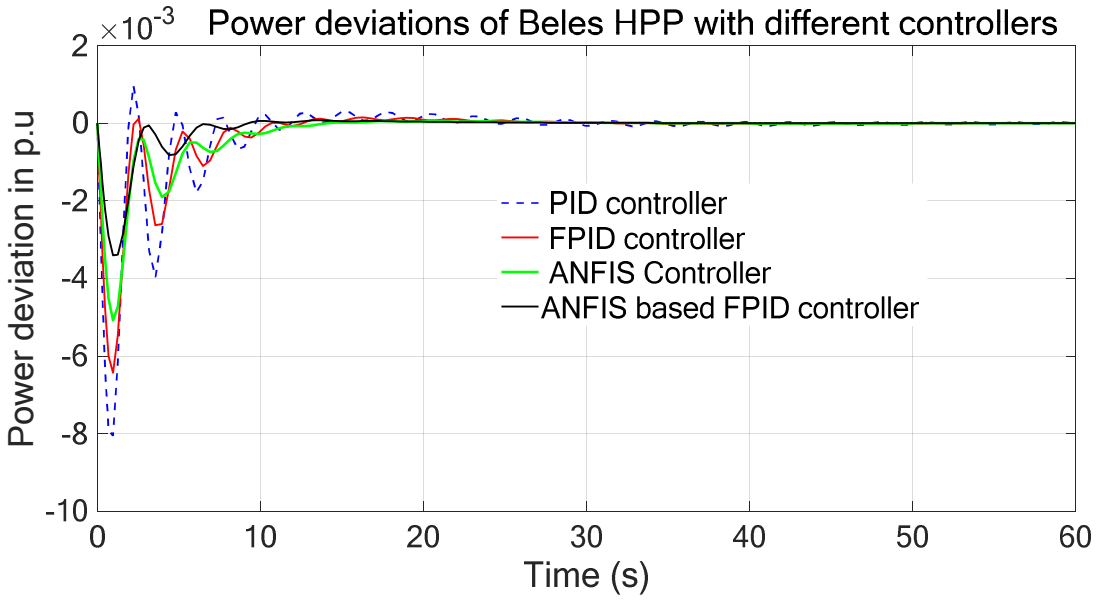
Table 6. Controller gain values and respective ITAE for a load disturbance in Area 1

	PID			FPID			ANFIS			ANFIS-FPID		
Area	K_p	K_i	K_d	K_p	K_i	K_d	K_p	K_i	K_d	K_p	K_i	K_d
Area-1	0.121	0.279	0.221	2.011	3.001	0.775	2.956	1.215	0.466	3.419	1.196	0.423

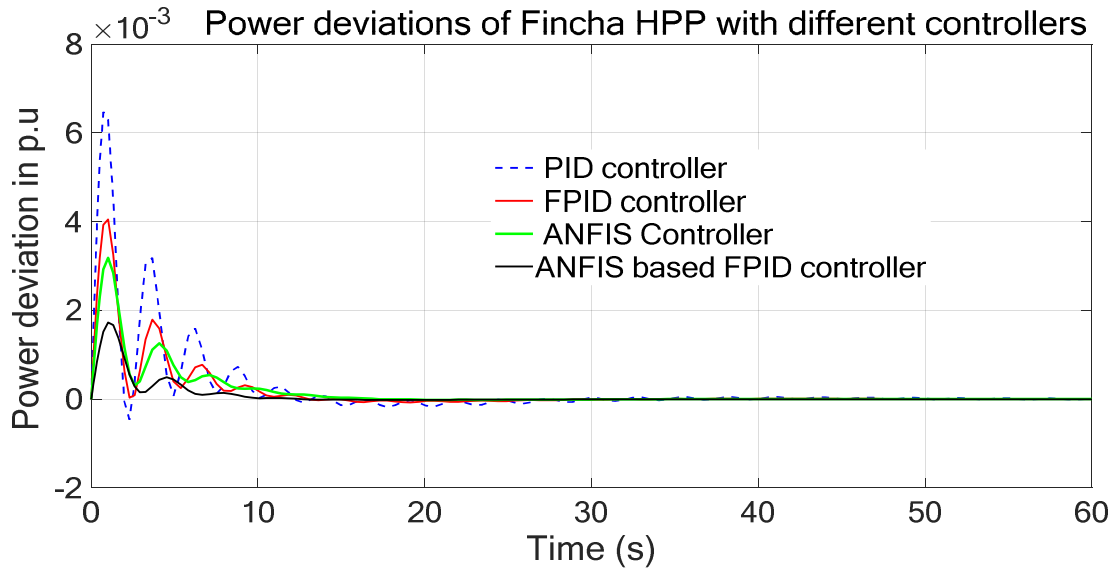
Area-2	0.146	0.029	0.035	2.096	1.988	0.665	3.013	2.553	0.662	3.774	2.675	0.651
Area-3	0.133	0.294	0.013	1.870	2.671	0.713	1.253	2.567	0.897	1.223	2.532	0.789
ITAE	0.0838			0.02636			0.00932			0.00565		

Comparative simulations demonstrate that in a single-area disturbance scenario, the hybrid controller reduced the frequency deviation settling time to 12.959 s with an ITAE of 0.00565, representing a substantial improvement compared to the 48.8824 s and ITAE of 0.0838 recorded for the existing PID system.

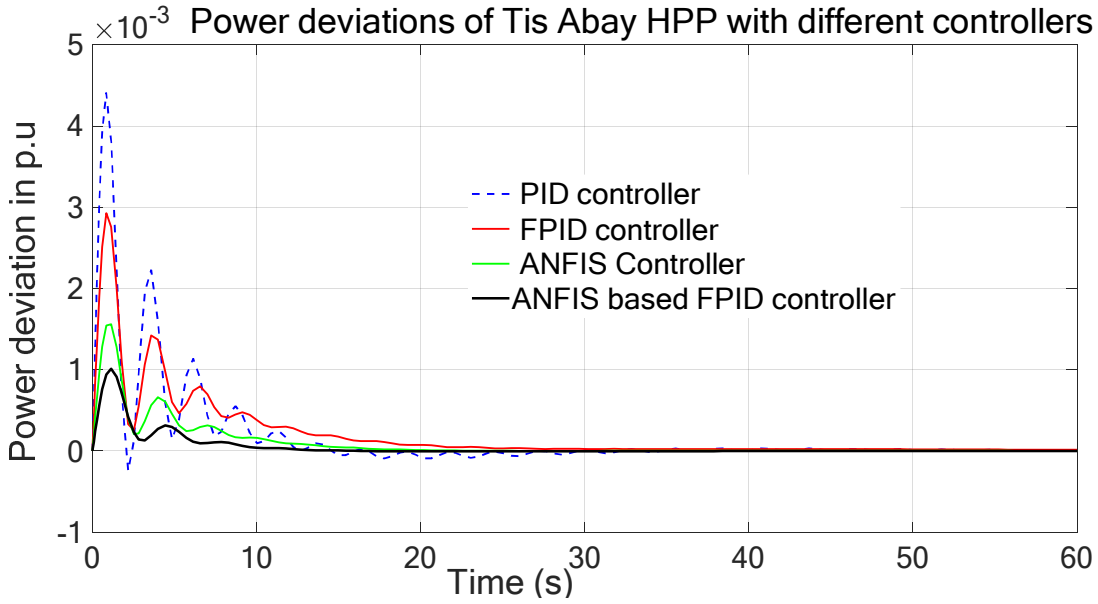
Fig. 17 shows the tie-line power deviation responses for the three areas following the 0.01 p.u. load disturbance in Area 1, with the corresponding comparative performance metrics presented in Table 7.



(a) area-1



(b) area-2



(c) area-3

Fig. 17: Tie-line power deviation responses for load disturbance in area one only

With PID, the peak tie-line power undershoot of -0.00805 p.u. corresponds to a 4.025 MW decrement at the 500 MW base. This deviation was reduced to -0.00339 p.u. (1.695 MW) with the ANFIS-based FPID controller. This improvement is attributed to the stable operating conditions in Areas 2 and 3 and the inherently better response of the electro-hydraulic governor in Area 1 to varying governor speed references.

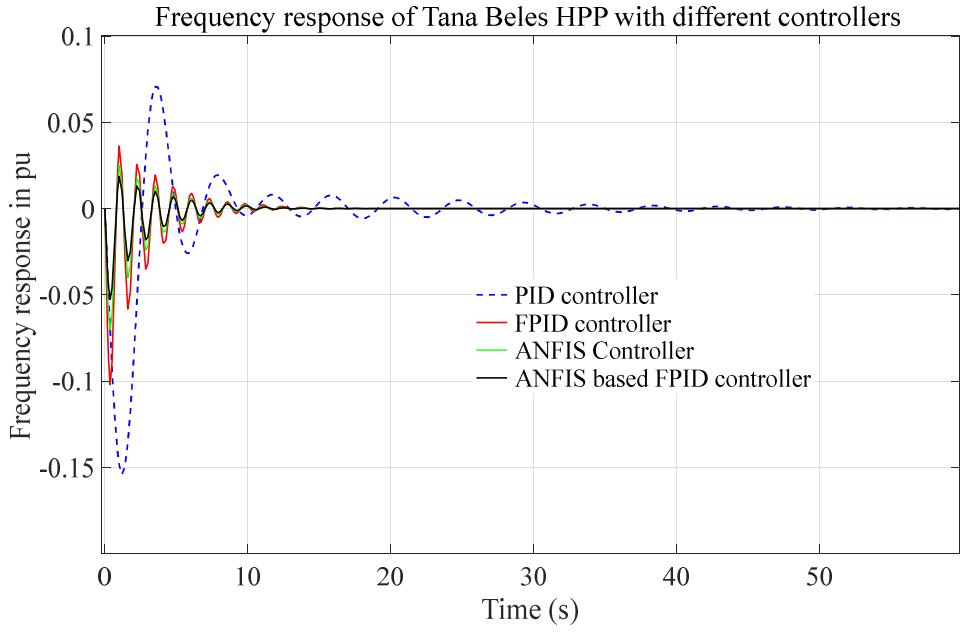
Table 7. Comparative analysis of tie-line power deviation responses for a load disturbance in Area 1.

Controllers	Performance Parameter	ΔP_{tie1}	ΔP_{tie2}	ΔP_{tie3}

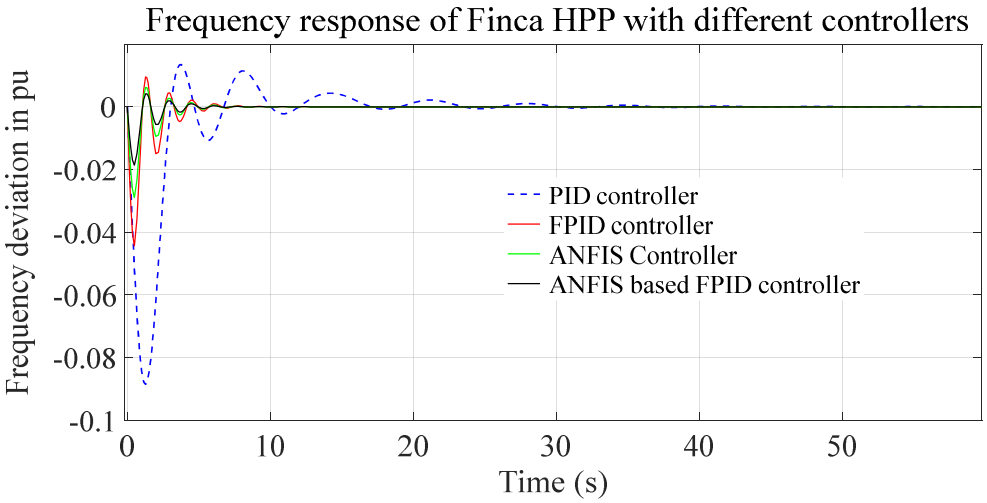
PID	Peak overshoot (pu)	0.00096	0.006470	0.00441
	Peak undershoot (pu)	-0.00805	-0.00046	-0.000243
	Settling time (s)	52.417	46.35	35.326
FPID	Peak overshoot (pu)	0.00011	0.00405	0.00293
	Peak undershoot (pu)	-0.0064	-0.00006	-0.000026
	Settling time (s)	25.7093	25.3829	27.5973
ANFIS	Peak overshoot (pu)	-0.00046	0.00318	0.00156
	Peak undershoot (pu)	-0.00508	-0.00001	-0.000018
	Settling time (s)	17.1925	16.344	16.267
ANFIS - FPID	Peak overshoot (pu)	-0.0006	0.001729	0.00101
	Peak undershoot (pu)	-0.0034	-0.00001	0.0000103
	Settling time (s)	14.285	13.1679	12.2452

4.2 Load Disturbance in All Areas

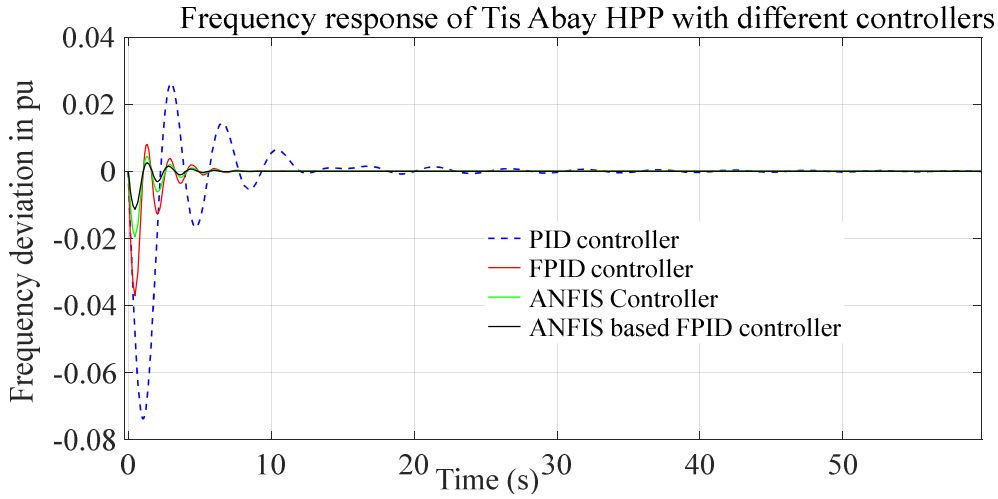
Scenario 2 involved simultaneous load increments of ΔPD1 = 0.46 p.u., ΔPD2 = 0.0268 p.u., and ΔPD3 = 0.016 p.u., corresponding to 50% load variation in Area 1 and 10% in Areas 2 and 3, to test controller performance and system stability under multi-area disturbances. The frequency deviation responses are shown in Fig. 18 and Table 8.



(a) for area-1



(b) for area-2



(c) for area-3

Fig. 18: Frequency deviation responses after load disturbances in all areas

Table 8. Comparative analysis of frequency deviation responses for simultaneous load disturbances in all areas

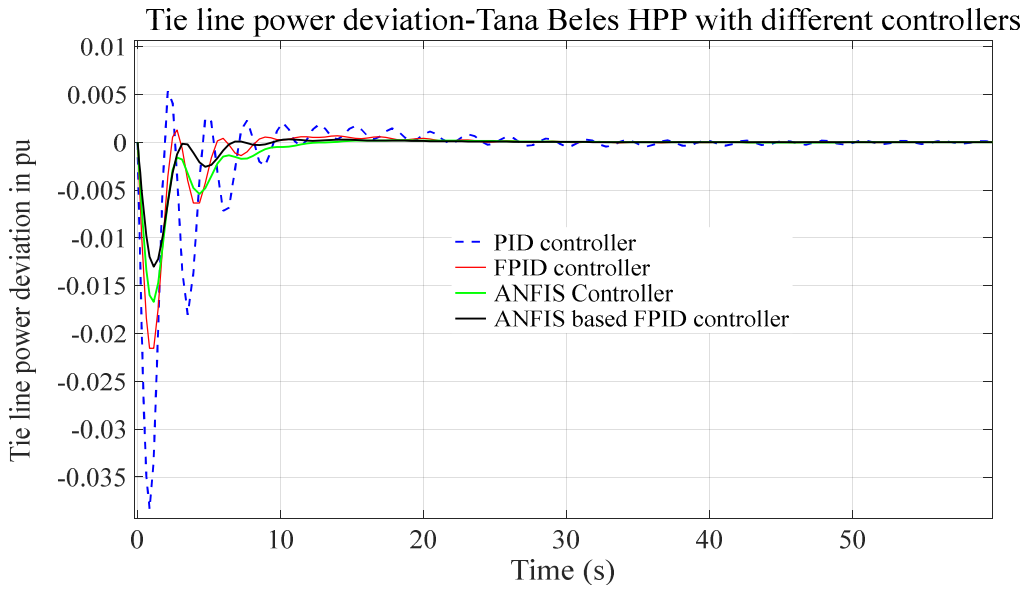
Controller	Performance Parameter	ΔF_1	ΔF_2	ΔF_3
PID	Peak overshoot (pu)	0.07080	0.01334	0.02627
	Peak undershoot (pu)	-0.15395	-0.08848	-0.07387
	Settling time (s)	59.890	53.326	51.413
FPID	Peak overshoot (pu)	0.036208	0.00954	0.00804
	Peak undershoot (pu)	-0.10191	-0.04437	-0.03716
	Settling time (s)	16.6929	14.985	13.256
ANFIS	Peak overshoot (pu)	0.024967	0.006214	0.004481
	Peak undershoot (pu)	-0.07028	-0.01857	-0.01961
	Settling time (s)	15.8112	13.901	13.112

ANFIS -FPID	Peak overshoot (pu)	0.01873	0.00417	0.002535
	Peak undershoot (pu)	-0.05271	-0.01493	-0.01136
	Settling time (s)	14.4515	12.880	12.328

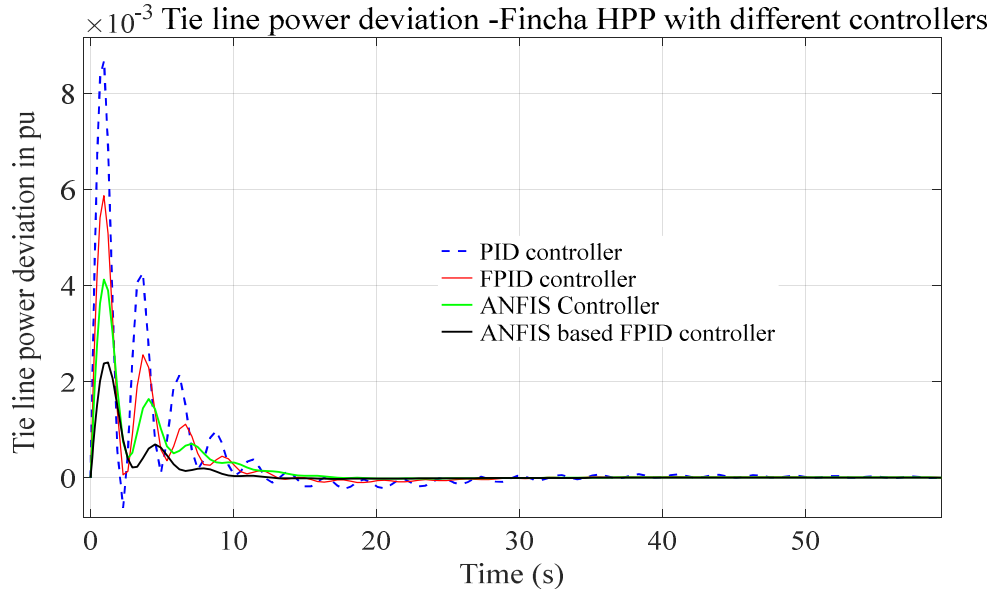
Under multi-area disturbances involving simultaneous load increments, the ANFIS-FPID model maintained its superiority by delivering the lowest ITAE of 0.02375 and consistently achieving smaller peak overshoots and undershoots across all control areas.

Table 9. Controller gain values and respective ITAE for simultaneous load disturbances in all areas

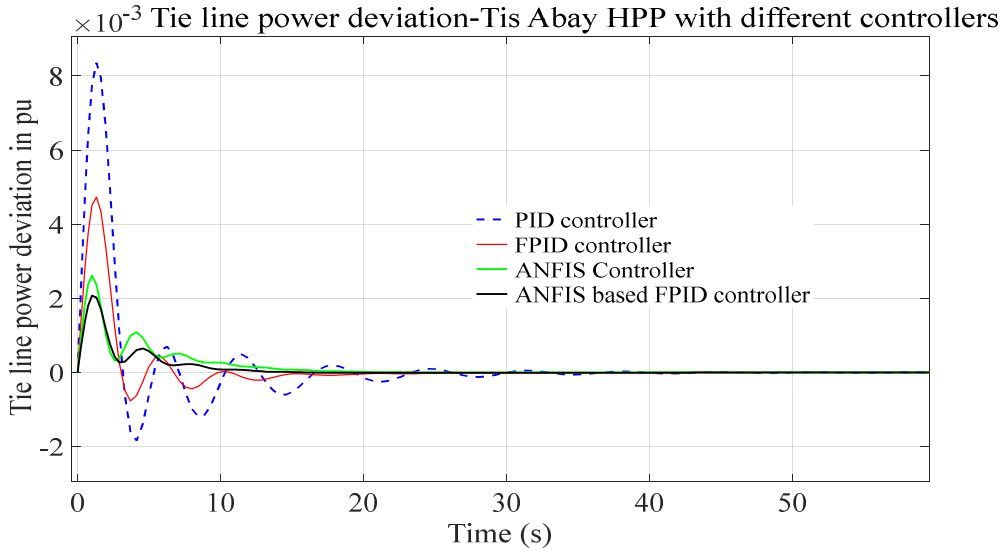
	PID			FPID			ANFIS			ANFIS-FPID		
Area	K_p	K_i	K_d	K_p	K_i	K_d	K_p	K_i	K_d	K_p	K_i	K_d
Area-1	0.783	0.801	0.776	1.991	1.878	0.892	1.896	1.902	0.908	2.02	1.82	1.131
Area-2	0.002	0.079	0.159	1.367	1.198	2.782	1.388	3.891	1.359	1.379	3.901	1.341
Area-	0.905	0.833	0.183	0.977	2.281	1.284	0.819	3.442	1.407	0.801	3.546	1.401
ITAE	0.97080			0.08119			0.04094			0.02375		



(a) for area-1



(b) for area-2



(c) for area-3

Fig. 19: Tie-line power deviation responses for all areas subjected to disturbances

Table 10. Comparative analysis of tie-line power deviation responses for simultaneous load disturbances in all areas

Controllers	Performance Parameter	ΔP_{tie1}	ΔP_{tie2}	ΔP_{tie3}
PID	Peak overshoot (pu)	0.00532	0.00868	0.00835
	Peak undershoot (pu)	-0.0336	-0.00062	-0.00183
	Settling time (s)	60.00	54.2550	48.6319
	Peak overshoot (pu)	0.00127	0.00587	0.00473

FPID	Peak undershoot (pu)	-0.02155	-0.00010	-0.00076
	Settling time (s)	27.6424	27.3259	24.0881
ANFIS	Peak overshoot (pu)	0.00013	0.00412	0.00240
	Peak undershoot (pu)	-0.01669	-0.00021	-0.00012
	Settling time (s)	24.4561	19.6142	17.7147
ANFIS - FPID	Peak overshoot (pu)	0.00026	0.002616	0.00208
	Peak undershoot (pu)	-0.01301	-0.00006	-0.00005
	Settling time (s)	21.3468	19.251	15.984

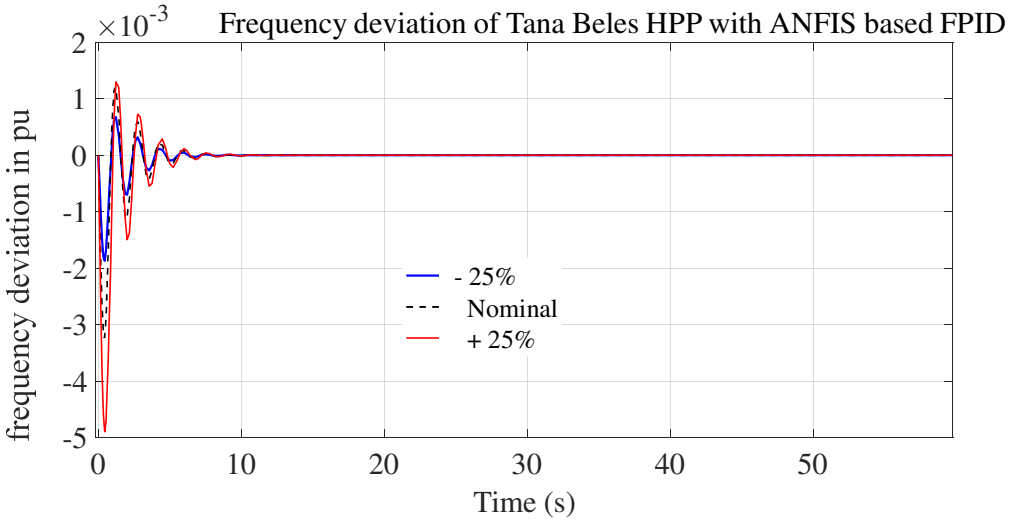
4.3 Robustness Analysis

The robustness analysis introduced a ±25% variation from nominal values for key system parameters, which is a standard benchmark in LFC studies. This test was applied specifically to the ANFIS-based FPID controller because it had previously demonstrated superior ITAE performance compared to the PID, FPID, and ANFIS controllers under nominal conditions. A 0.01 p.u. load disturbance, the standard value commonly used for testing LFC robustness [20], was applied to Area 1 only. The parameter variations considered are listed in Table 11.

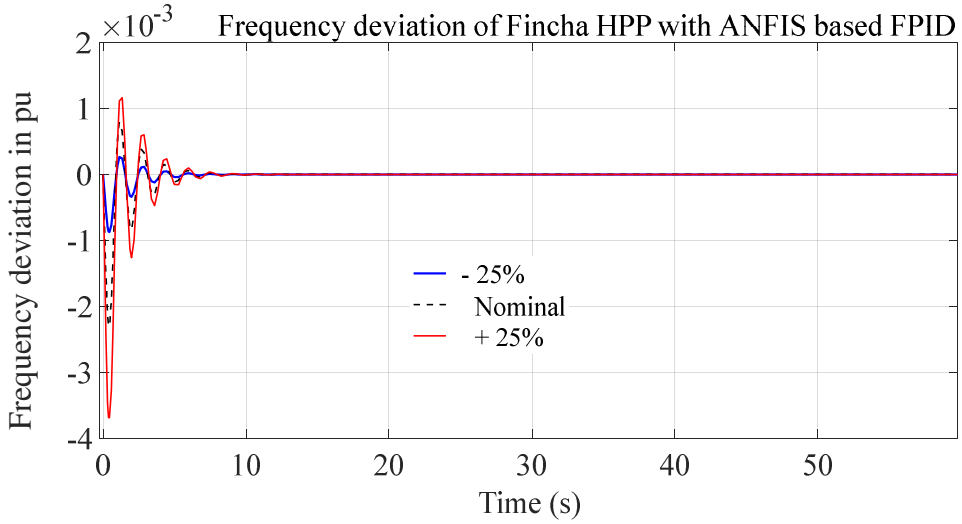
Table 11. Parameter values for robustness analysis of the proposed controller

Parameter	-25%	Nominal value	+25%
T_{g1}	3.75	5	6.25
T_{g2}	4.5	6	7.5
T_{g3}	4.5	6	7.5
T_{w1}	1.3125	1.75	2.1875
T_{w2}	1.5	2	2.5
T_{w3}	1.5	2	2.5
H_1	2.355	3.14	3.925
H_2	2.28	3.04	3.8
H_3	1.875	2.5	3.125
R_1	0.0375	0.05	0.0625
R_2	0.03	0.04	0.05
R_3	0.03	0.04	0.05

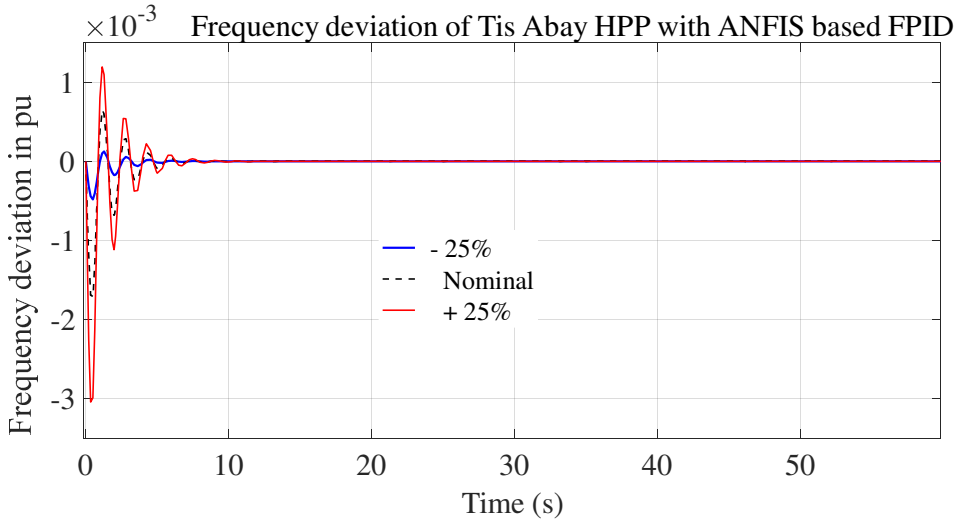
Fig. 19 presents the frequency deviation responses for the robustness analysis using the ANFIS-based FPID controller, where the blue lines represent the response at -25% parameter variation, the dotted black lines represent the nominal response, and the red lines represent the +25% response. The results demonstrate the controller's ability to maintain stability and performance despite significant uncertainties in system parameters.



(a) for area-1



(b) for area-2



(a) for area-3

Fig. 20: Frequency deviation responses for robustness analysis with ANFIS based FPID controller

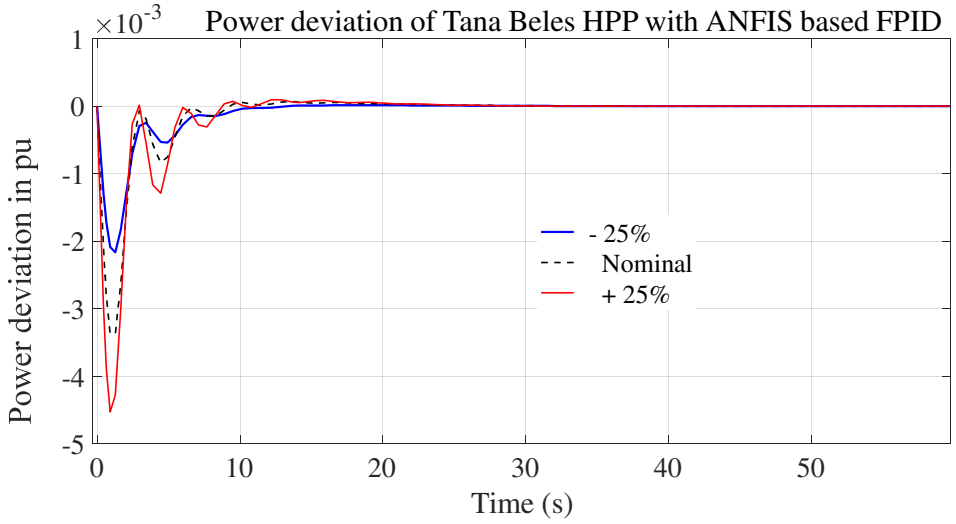
Table 12. Comparative robustness analysis of frequency deviation responses using the ANFIS-based FPID controller

Controller	Performance Parameter	ΔF_1	ΔF_2	ΔF_3
-25%	Peak overshoot (p.u)	0.00068	0.00026	0.00013
	Peak undershoot (p.u)	-0.00187	-0.00369	-0.00048
	Settling time (s)	11.005	10.201	9.857
Nominal	Peak overshoot (p.u)	0.00120	0.00081	0.00064
	Peak undershoot (p.u)	-0.00325	-0.00231	-0.00178
	Settling time (s)	13.959	12.927	12.283
+25%	Peak overshoot (p.u)	0.00129	0.00116	0.0064
	Peak undershoot (p.u)	-0.004894	-0.00369	-0.00171
	Settling time (s)	14.201	13.911	13.872

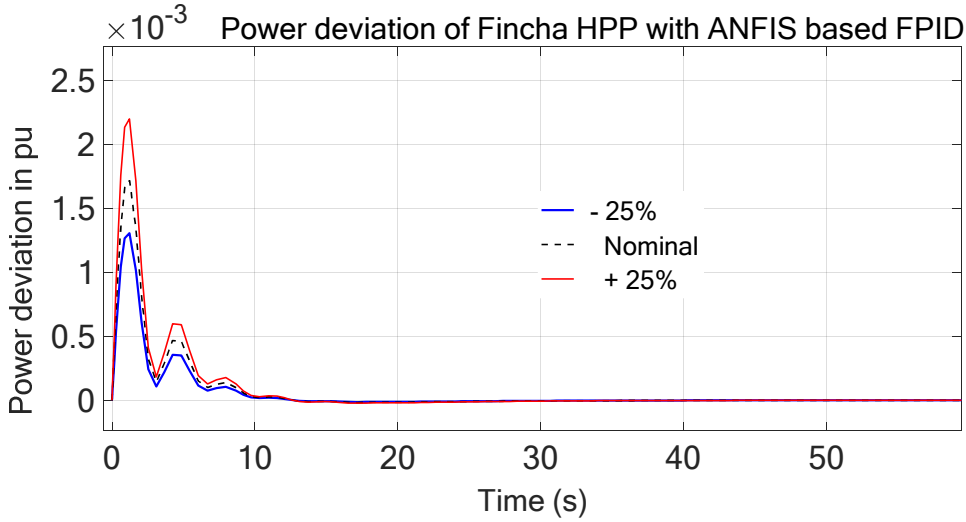
Table 13. Controller gain values and respective ITAE for robustness analysis

	Gain	-25%	Nominal	+25%
Area-1	K_p	2.091	3.419	3.191
	K_i	2.038	1.196	0.906
	K_d	0.23	0.423	0.594
Area-2	K_p	4.294	3.774	3.697
	K_i	2.253	2.675	2.384
	K_d	0.331	0.651	0.739
Area-3	K_p	0.492	1.223	0.566
	K_i	0.502	2.532	0.431
	K_d	-0.0693	0.783	0.022

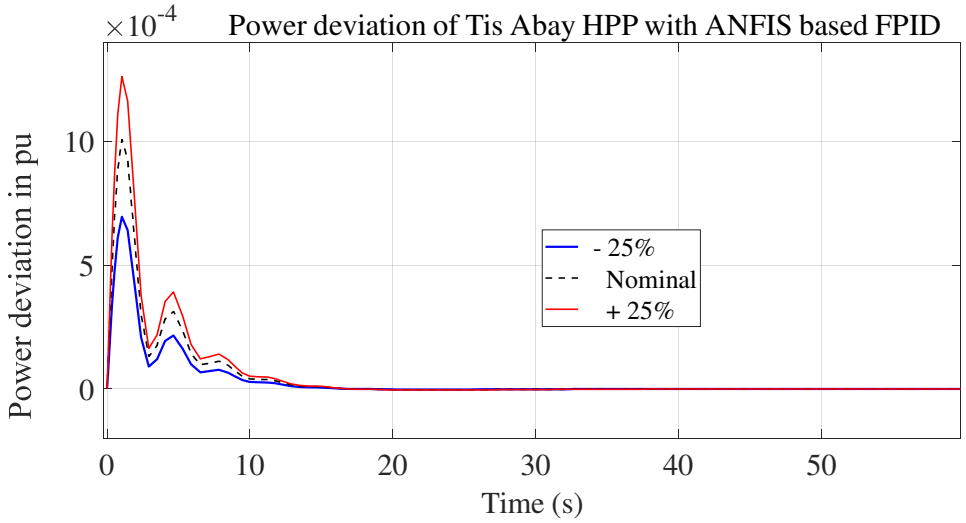
ITAE	0.00541	0.00565	0.00580



(a) for area-1



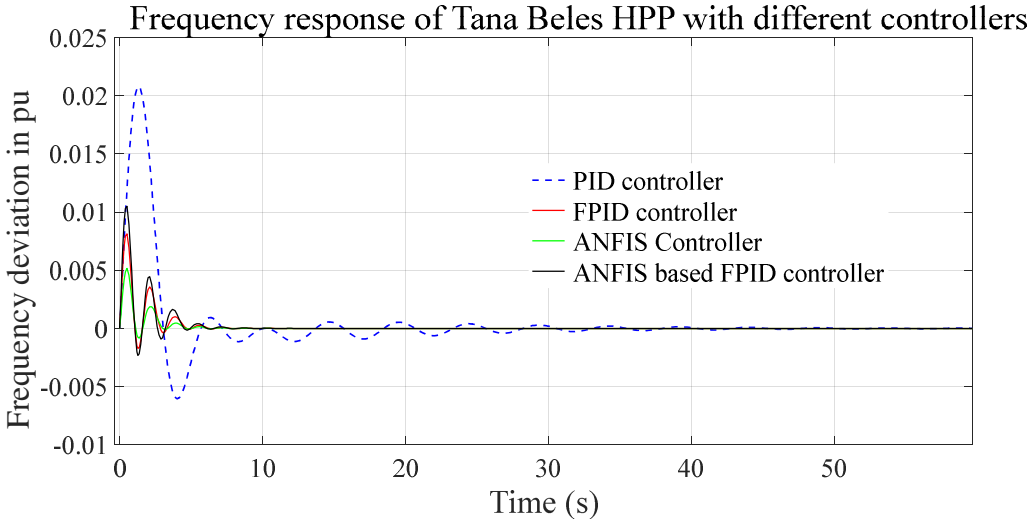
(b) for area-2



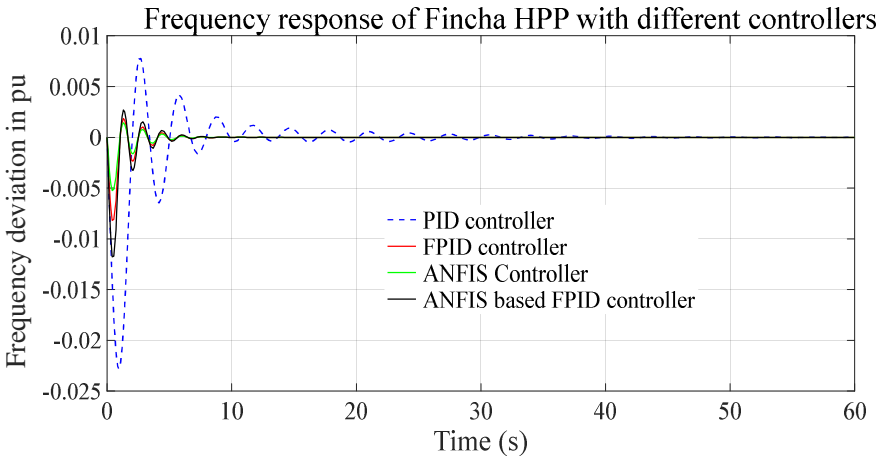
(c) for area-3

Fig. 21: Tie-line power deviation responses for robustness analysis with ANFIS based FPID controller

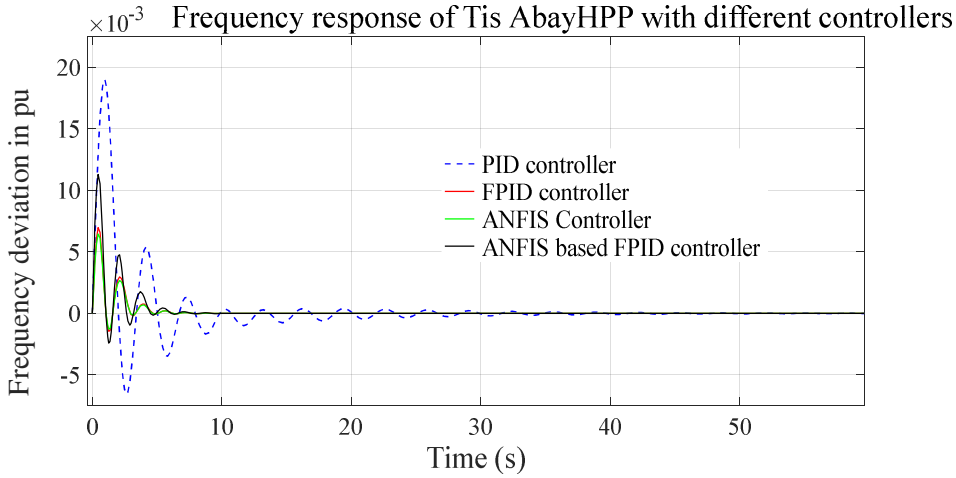
The performance of the controller was tested under load disturbance conditions. Figure 23 illustrates the system's frequency response, depicting the frequency deviation resulting from both load increments and decrements. Specifically, the frequency deviations for all areas presented for the case study with the following load changes: ΔPD1 = -0.01 pu. (decrement), ΔPD2 =+0.01 pu. (increment), and ΔPD3 =-0.01 pu. (decrement).



(a) for area-1



(b) for area-2



(c) for area-3

Fig. 22: Frequency deviation versus time plot for system disturbance by load increment and decrement

The proposed hybrid ANFIS-based FPID controller demonstrated significant performance improvements across all evaluated scenarios, summarized as follows:

- Settling Time Improvement (Scenario 1): The proposed controller reduced the frequency deviation settling time by approximately 73.5%, from 48.8824 s with PID to 12.959 s.
- ITAE Reduction (Scenario 1): The ITAE was reduced by over 93%, from 0.0838 for PID to 0.00565 for the hybrid model.

- Tie-Line Power Performance: The peak tie-line power undershoot in Area 1 was reduced by nearly 58%, from -0.00805 p.u. (4.025 MW) with PID to -0.00339 p.u. (1.695 MW).
- Robustness Under Multi-Area Disturbances (Scenario 2): The ANFIS-FPID delivered the lowest ITAE of 0.02375, approximately 97.5% lower than the PID's ITAE of 0.97080.
- Parameter Sensitivity Stability (Scenario 3): The system remained stable with an ITAE range of only 0.00541 to 0.00580 under ±25% parameter variations.

5. Challenges and Limitations

While this paper demonstrates that the ANFIS-based FPID controller can significantly improve frequency and tie-line power deviations in the Northwest Region of the Ethiopian power grid, Ethiopia's NLDC will face substantial computational, real-time, and human resource challenges in deploying such controllers. The inherent computational burden of ANFIS, including high computational cost and susceptibility to the curse of dimensionality when handling multiple complex inputs, raises questions about its real-time feasibility in a dynamic grid environment where rapid, millisecond-level responses to disturbances are critical. In addition, infrastructural and human resource constraints, including a shortage of skilled control system professionals, limited access to high-quality real-time operational data for training robust models, and the costs associated with upgrading hardware and specialized software, would delay implementation.

Although the paper demonstrates the technical superiority of the hybrid ANFIS-based FPID controller, several main limitations regarding its implementation scope have been identified. Non-linear constraints such as governor dead band (GDB) and generation rate constraints (GRC), as well as the integration of wind and thermal power plants into the model, were not

included, and validation was limited to MATLAB/Simulink simulation. Furthermore, the LFC model is restricted to a three-area hydropower system and does not yet incorporate all hydro, thermal, and wind plants. Cybersecurity risks and requirements for upgrading the existing communication protocols of Ethiopia's NLDC were also not considered.

6. Conclusion and Recommendations

6.1 Conclusion

This study designed an ANFIS-FPID LFC controller for the Northwest Region of the Ethiopian power grid, represented by a three-area LFC model, and compared its performance with conventional PID, FPID, and ANFIS controllers. Although PID serves as the existing primary LFC mechanism, the proposed ANFIS-based FPID is intended to serve as a supplementary LFC mechanism that enhances the existing primary control capability and enables centralized operation. Performance was evaluated under three scenarios: a 0.01 p.u. disturbance in Area 1, simultaneous disturbances across all areas (0.46 p.u., 0.0268 p.u., and 0.016 p.u.), and a sensitivity analysis with ±25% parameter variations. Results confirmed that the ANFIS-FPID controller consistently achieved shorter settling times, lower overshoots, and reduced undershoots compared to all other controllers, while maintaining robustness under parameter changes.

By combining ANFIS's adaptive learning capability with FPID's nonlinear handling ability, the hybrid controller effectively manages uncertainties and dynamic conditions. This represents a significant advancement over conventional PID mechanisms and offers a resilient solution for grid stability and frequency regulation in Ethiopia’s interconnected power system.

Based on these conclusive findings, the ANFIS-based FPID controller outperforms the existing PID mechanism. Ethiopian Electric Power (EEP) is therefore recommended to pilot this controller and implement a centralized LFC mechanism to enhance national grid resilience, prevent blackouts, and protect infrastructure through real-time monitoring. The adoption of

such intelligent controllers would enable real-time adaptation to the grid's fluctuating energy landscape without the need for manual retuning. However, the deployment of this technology requires strategic investment in modernization, including the upgrading of communication protocols at the NLDC and specialized training for engineers in AI-driven control systems. This framework provides a technically viable pathway for Ethiopia to enhance its grid reliability and successfully integrate future renewable energy expansions.

6.2 Future Work

Three priority directions for future work are recommended. First, practical validation should be pursued by transitioning to Hardware-in-the-Loop (HIL) testing to ensure the ANFIS-based FPID controller can handle real-time execution and PID parameter tuning. Second, the model should be modernized by integrating large-scale renewable energy sources such as the existing wind and thermal power plants, while expanding the network to include four or more regions to better reflect the complexity of the evolving Ethiopian grid. Third, system realism should be enhanced by incorporating non-linear operational constraints such as governor dead band (GDB) and generation rate constraints (GRC), alongside investigations into cybersecurity risks of AI-based LFC and integration with NLDC-SCADA systems.

Declarations

Funding: The authors declare no funding for this research.

Data availability: The datasets generated and/or analysed during the current study are not publicly available but are available from the corresponding author on reasonable request.

Competing Interests: The authors declare that they have no competing interests.

Conflicts of Interest: The authors declare that they have no conflict of interest.

Ethics and Consent to Participate: Not applicable.

Consent to Publish: All authors consent to the publication of this paper.

Acknowledgements: The authors express their sincere gratitude to the Bahir Dar Institute of Technology, Bahir Dar University, Dr. Girmaw Teshager Bitew, and Mr. Yechale Amogne Alemu (MSc) for providing the opportunity to conduct this research and for their valuable guidance throughout.

Appendix

Table A. Transmission line reactance data.

From	To	Length	Line X (Ω)	Xeq (pu)
Fincha	Debre-Markos	95.15	40.2853	0.1259
Bahir-Dar-2	Tana Beles	62.84	19.4541	0.06079
Bahir-Dar-2	Debre-Markos	193.73	63.7763	0.1993
Tis- Abay-2	Bahir-Dar-2	29.00	2.0446	0.0064
Fincha	Tis Abay-2	317.88	106.1062	0.3316
Tana Beles	Fincha	351.72	123.5157	0.3860
Tana Beles	Tis Abay-2	91.84	21.4987	0.0672

Note: Tana Beles, Fincha, and Tis Abay-2 are the hydropower plants in NWREEP representing Areas 1, 2, and 3, respectively; Debre-Markos and Bahir Dar-2 are substations located between the control areas.

Table B. Nominal voltage level, generation capacity, and system parameters.

Power plant	V Nominal Voltage KV	S in (MVA)	H Inertia in sec	B Frequency Bias constant,	Angles δi0 (radians)	Number of Generators	Installed capacity, MW
Tana Beles	15	532	3.14	0.425	-0.32	4	460
Fincha	13.8	140	3.04	0.425	-0.382	4	134
Tis Abay-2	10.5	80	2.5	0.425	-0.402	2	73

Table C. Governor, turbine, and generator parameter values for Tana Beles and Fincha HPP.

Power plants	R, Permanent Drop	R_T, Temporary drop	T_g Main governor Time Constant	T_1 Speed governor reset time,	T_2 Transient droop time constant,	T_w water time constant	D Turbine damping	f Rated frequency Hz
Tana Beles	0.05	0.4	5	10	0.5	1.75	0.4	50
Finch	0.04	0.5	6	10	0.5	2	0.3	50
For Tana Beles Pilot valve and servo time constant, Tp=0.05								

Note: For Tana Beles, the pilot valve and servo time constant is Tp = 0.05 s.

Table D. Control parameters for the HYGOV hydraulic governor of Tis Abay-2.

Tis Abay-2 HYGOV Parameters	
R, Permanent drop	0.04
r, temporary drop	0.5
Tr (>0) governor time constant	6
Tf (>) filter time constant (equal to pilot valve and servo time constant, Tp)	0.05
Tg (>0) servo time constant (main governor servo time constant)	0.5
Tw	2.0

Table E. Transmission line synchronizing coefficients.

From	To	Length (Km)	T Transmission line constant value	T Transmission line constant Naming
Tana Beles	Fincha	351.7	0.004	T_{12}
Fincha	Tana Beles	351.7	-0.012	T_{21}
Tana Beles	Tis Abay-2	91.84	0.016	T_{13}
Tis Abay-2	Tana Beles	91.84	-0.101	T_{31}
Fincha	Tis Abay-2	317.85	0.010	T_{23}
Tis Abay-2	Fincha	317.85	-0.018	T_{32}

References

[1] A. A. Khan, "Fuzzy PID Controller: Design, Tuning and Comparison with Conventional PID Controller."

[2] S. Berwal and B. Singh, "Load Frequency Control of a Renewable Source Integrated Four Area Power System using Hybrid Controller," International Research Journal of Engineering and Technology, 2019.

[3] R. Fagna, "Load Frequency Control of Single Area Thermal Power Plant Using Type 1 Fuzzy Logic Controller," Science Journal of Circuits, Systems and Signal Processing, vol. 6, no. 6, p. 50, 2017.

[4] C. M. Reddy and A. S. Kumar, "Load Frequency Control of Deregulated Power System Using Different Fuzzy Controllers," 2013.

[5] C. S. A. Soundarrajan and Dr. S. Sumathi, "Particle Swarm Optimization Based LFC and AVR of Autonomous Power Generating System," IAENG International Journal of Computer Science, 37:1, 2010.

[6] A. Ikhe and A. Kulkarni, "Load Frequency Control for Two Area Power System Using Different Controllers," 2013.

[7] V. Kumar and A. Patra, "Application of Ziegler-Nichols Method for Tuning of PID Controller," International Journal of Electrical and Electronics Engineers, 2016, pp. 559–570.

[8] E. Gholampour, "Load frequency control based on optimized type-1 fuzzy controller," vol. 2, pp. 24–31, 2013.

[9] M. F. A. Limon et al., "Grey wolf optimization-based fuzzy-PID controller for load frequency control in multi-area power systems," Journal of Automation and Intelligence, 2025.

[10] Z. Qu, W. Younis, Y. Wang, and P. M. Georgievitch, "A Multi-Source Power System's Load Frequency Control Utilizing Particle Swarm Optimization," Energies, vol. 17, no. 2, Jan. 2024, doi: 10.3390/en17020517.

[11] B. Sokke Rameshappa and N. M. Shadaksharappa, "Neuro-Fuzzy Intelligent Controller for LFC of a Four-Area Power System," International Journal of Engineering Technologies and Management Research, vol. 9, no. 10, pp. 50–60, Oct. 2022, doi: 10.29121/ijetmr.v9.i10.2022.1235.

[12] D.-V. Doan, K. Nguyen, and Q.-V. Thai, "Load-Frequency Control of Three-Area Interconnected Power Systems with Renewable Energy Sources," 2022.

[13] D. Sharma, "Automatic generation control of multi-source interconnected power system using adaptive neuro-fuzzy inference system," International Journal of Engineering, Science and Technology, vol. 12, no. 3, pp. 66–80, Sep. 2020, doi: 10.4314/ijest.v12i3.7.

[14] R.-E. Precup, A.-T. Nguyen, and S. Blažič, "A survey on fuzzy control for mechatronics applications," Int. J. Syst. Sci., vol. 55, no. 4, pp. 771–813, 2024.

[15] P. Kundur, Power Systems Stability and Control. University of Toronto, Toronto, Ontario: McGraw-Hill Inc., 1994.

[16] P. Kumar Yadav, D. Bhasker, and S. Kumar Upadhyay, "Load Frequency Hybrid Intelligent Control for Multi-Area Interconnected Power System," International Journal of Electrical Engineering and Technology, vol. 12, no. 10, pp. 12–22, 2021.

[17] A. Mengesha, "Peak Load Shaving and Ancillary Support of Distribution Substation Using Grid Connected Optimized Solar Photovoltaic System," Bahir Dar University, Bahir Dar, 2024.

[18] X. Yu, J. Zhang, C. Fan, and S. Chen, "Stability analysis of governor-turbine-hydraulic system by state space method and graph theory," Energy, vol. 114, pp. 613–622, 2016.

[19] D. H. Ngoma, A. Mfangavo, and B. Masenga, "Comparative control governor systems for power and frequency optimization of an islanding off-grid small hydropower plant," Discover Energy, vol. 5, no. 1, p. 6, 2025.

[20] B. Singh and S. Krishan Bishnoi, "An Application of ANFIS-PID Controller for Multi Area Hybrid Power System," in Artificial Intelligence and Communication Technologies, Soft Computing Research Society, 2023, pp. 613–627. doi: 10.52458/978-81-955020-5-9-59.